Part II

A Continuum Mechanical Theory for Avalanches Down Non-Trivial Topographies

Chapter 3

A Continuum Mechanical Theory for Granular Avalanches

3.1 General Introduction

It is probably fair to state that SAVAGE & HUTTER [112], in 1989, developed the first *continuum mechanical theory*, abbreviated in this thesis by "SH-theory", capable of describing the evolving *geometry* of a finite mass of a granular material and the associated *velocity* distribution as an avalanche slides down inclined surfaces. Their model provides a more *complete analysis* of such flows than previous models have done, and its extension as well as comparison with laboratory experiments demonstrate it to be *largely successful*. This depth-averaged hydraulic model is one of the most sophisticated and widely used models by today's practitioners. The reason for this is that the SH-model is simple to understand and very economical to implement even to extremely huge natural phenomena like avalanches and debris flows. Another *very important feature* of the model is that it is based on *physical reasoning* and *rigorous mathematical foundations*. Equally important is the fact that the model is *scale invariant* and that it can predict the dynamics of the flow of granular material quite well in chemical and process engineering as well as geophysical circumstances. Several simplifying, but nevertheless realistic, assumptions were made that streamlined the mathematical formulation. They are as follows:

- The moving mass was supposed to be *volume preserving*. This assumption is based on observations in the laboratory that possible volume expansions and compactions arise at the initiation and still stand, whilst during its motion the moving mass is nearly preserving its volume. Since the dynamics define the motion, supposing volume preserving is an adequate approximation.

- The moving and deforming *dry* granular mass is *cohesionless* and obeys a MOHR-COULOMB *yield criterion* both inside the deforming mass as well as at the sliding basal surface, but with different internal, ϕ, and bed, δ, friction angles. This assumption is based on the experimental fact that on any plane, at which shear and normal traction may act, their ratio is constant and equal to the tangent of ϕ or δ, respectively. This classical criterion is quite appropriate for materials with rate independent constitutive properties.

- The avalanching body is assumed to be *stress-symmetric* and the shear stresses

lateral to the main flow direction can be neglected.

- The body is supposed to be in an *isothermal* state.

- The *geometries* of the avalanching masses are *shallow* in the sense that typical avalanche thicknesses are small in comparison to the extent parallel to the sliding surface. This assumption allows introduction of a shallowness parameter and simplification of formulas in terms of it.

- The avalanching motion consists of shearing within the deforming mass and sliding along the basal surface. However, on the basis of observations the shearing deformation commonly takes place within a very small basal boundary layer that it is justified to collapse this boundary layer to zero thickness and to combine the sliding and shearing velocity to a single sliding law with somewhat larger modelled *sliding velocity*. This then effectively means that variations of the material velocities across the thickness may be ignored and thickness-averaged equations may be employed. This is a method introduced by VON KÁRMÁN [128] and later refined by POHLHAUSEN [91], in which the equations are averaged over depth and the velocity profile is assumed.

- In order to obtain a spatially reduced theory for the flow down a slope of constant inclination angle, the leading order two-dimensional equations are *integrated through the avalanche depth*.

- *Scaling analysis* identifies the physically significant terms in the governing equations and isolates those terms that can be neglected. The assumptions of the theory are formally stated in a Theorem in Section 3.3.3.

This simple spatially one-dimensional model, applicable along a straight sliding surface, has been generalised in various different ways. In fact, one of the strengths of the procedure is that the model can be generalised to higher dimensions, to more complex geometries and for multi-phase flows like debris and pyroclastic-flows, see [17, 31, 32, 34, 35, 49, 55, 56, 57, 87, 90, 98, 99, 100, 101, 102, 103, 104, 112, 113]. A generalisation to flows along simple curved basal topography was performed in 1991 [113] in order to obtain complete knowledge of the avalanche motion from initiation on a steep slope to run-out on a shallow slope. The coordinates were generated by a basal curve following the direction of steepest decent and assuming no topographic variations perpendicular to it. This led to an orthogonal metric and a description of the motion that predominantly singles out the talweg direction. This allowed the local inclination angle to vary as a function of the downslope coordinate.

3.2 Generalisations of the Original Theory

There are two main streams of development of this theory depending on the coordinate system and the topography. The main attention has been focused on different topographic structures. In the following discussion we will consider both of them separately.

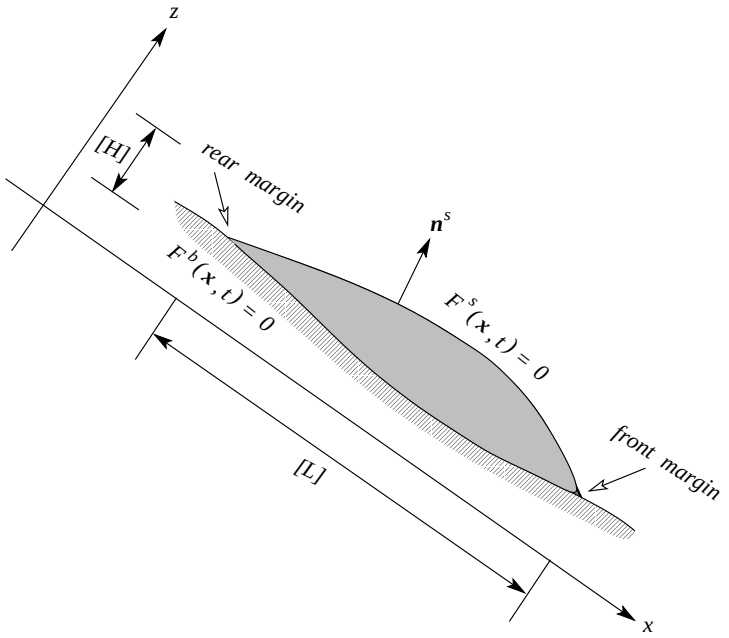

Figure 3.1: Sketch of the geometry of a finite mass of granular material moving along a curved rigid bed showing the definition of the free surface given by $F^s(\mathbf{x}, t) = 0$ and the equation of the bed $F^b(\mathbf{x}, t) = 0$. Also indicated are the scales $[L]$ and $[H]$ for the spread and the maximum height of the avalanche, and the free surface unit normal $\mathbf{n}^s$ pointing outward from the body

3.2.1 With Respect to the Coordinate System

The original paper of Savage & Hutter [112] was based on a formulation using Cartesian coordinates. This initial investigation considered the idealised problem of a finite mass of granular material released from rest on a rough inclined plane. Consider now free surface flow of a granular material along a slowly varying bottom topography as shown in Fig. 3.1. When the underlying topography varies moderately along the longitudinal direction but has no variation in the transverse direction, a treatment using Cartesian coordinates is likely a first good approximation of the problem. However, in many situations the downslope variation of the topography may deviate strongly from a straight line. In such cases it is quite natural and convenient to adopt a coordinate system that can better describe the topography of the base of the flowing material. In a second stage of the development of their theory Savage & Hutter, in 1991, [113] wrote a paper that describes a model predicting the flow of an initially stationary mass of cohesionless dry granular material down rough curved beds, see Fig. 3.2. By depth integration of the incompressible conservation of mass and linear momentum equations that were written in terms of a curvilinear coordinate system aligned with the curved bed, evolution equations for the depth h and the depth-averaged velocity u were obtained. In this way, the bed curvature effects, in the longitudinal direction, were incorporated in the theory. Such a curvilinear coordinate system, for instance, can adequately describe a chute having a bed made up of a straight inclined portion followed by a curved part and a horizontal portion. In all subsequent developments and extensions of the SH-theory for confined and unconfined chutes, two-dimensional and three-dimensional flows the basal topographies were modelled by using curvilinear coordinate systems in a natural way, and all equations of motion were written in such appropriate coordinate form.

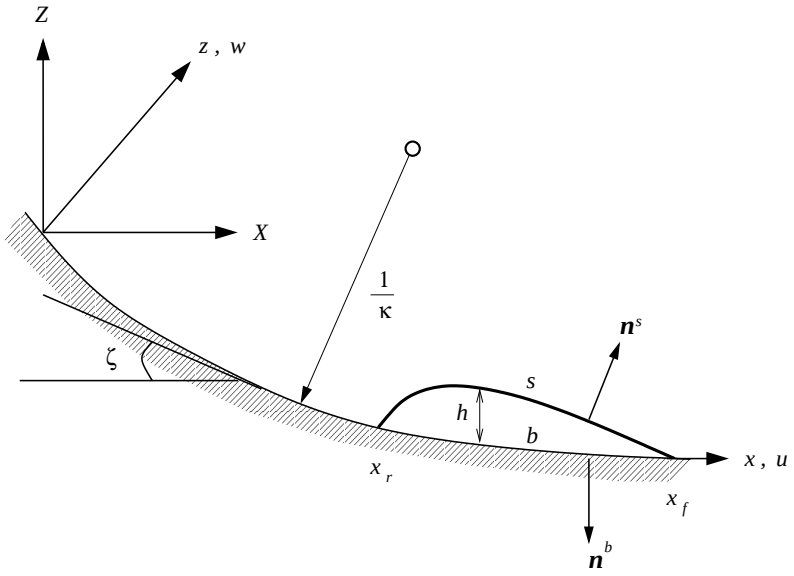

Figure 3.2: Definition sketch of the coordinate system and geometry of a finite mass of granular material moving down a rough curved rigid bed. Here, x, z are curvilinear coordinates in the direction of the flow and normal to the bed, whereas X, Z are their Cartesian counterparts. u and w are the velocity components along the x and z coordinates. x_f and x_r indicate the front- and rear-margins, whilst s, b and h are the free- and basal-surfaces and the height of the moving and deforming avalanche on a rough bed whose local inclination angle with the horizontal is ζ and the local radius of curvature is κ. Also shown are the free-surface and basal unit normals pointing outwards from the avalanching body

3.2.2 With Respect to the Basal Topography

a) One-Dimensional

The major part of the extensions of the original SH-theory [112] is concerned with the basal topography on which the flow of cohesionless incompressible granular avalanches take place. As described earlier, the first theory was developed for flow along a rough *inclined plane* or a situation in which the main flow direction is nearly parallel to such a plane, as shown in Fig. 3.1. The theory was immediately [113] extended to a two-dimensional *curved bed* which could better predict the flow of an avalanche on a slightly curved topography. Savage & Hutter studied the two-dimensional motion of a pile of granular material as it starts from rest and flows down a rough bed. The bed is assumed to have a steep slope at the initial position of the pile and is curved so as to approach a horizontal flat in the downstream direction. It is convenient to introduce curvilinear coordinates x and z as shown in Fig. 3.2. The x-coordinate, i.e., the coordinate line $z = 0$, follows the basal profile and the coordinate lines $x = \text{const.}$ are straight rays perpendicular to the basal profile. There are some restrictions of application of this coordinate system. It possesses a singularity at all centers of the curvature where z equals the radius of curvature. Physically, these points correspond to the positions at which consecutive z-axes (which vary locally) intersect with one another. Therefore, in applications we require that the avalanche does not pass through one of these points during the course of its motion, see Fig. 3.3.

Hutter & Koch [47] successfully implemented the theory for curved channels to the motion of granular avalanche in an exponentially curved and two- dimensionally confined

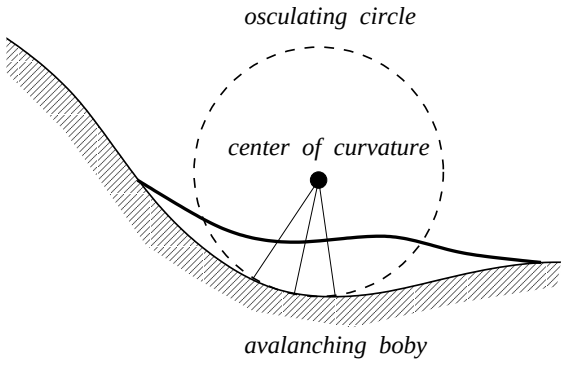

Figure 3.3: The avalanching body is not passing through the center of curvature of the basal surface. The center of curvature is the point of singularity of the coordinate system under consideration

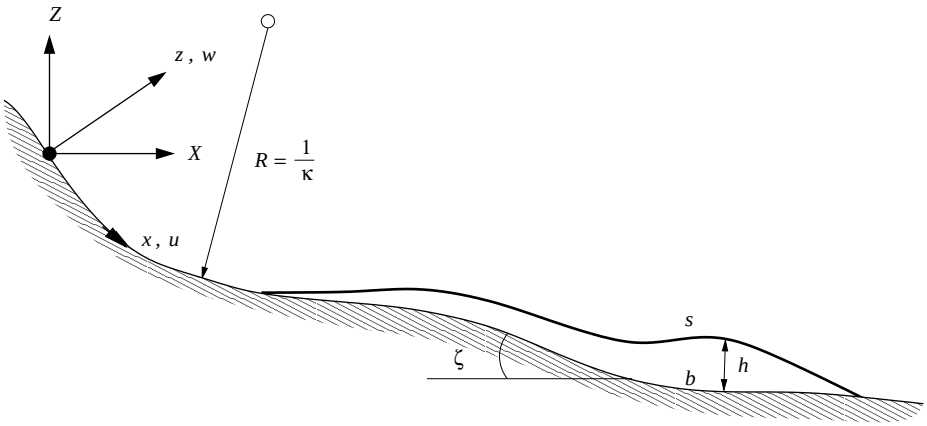

Figure 3.4: Same as in Fig. 3.2 but for a convex and concave chute

chute. Greve & Hutter [34] subsequently extended the implementation of such a theory of curved beds to a motion of an avalanche in a convex and concave chute, see Fig. 3.4. Because of the bump and depending upon the granulate-bed combination an initial single pile of the granular body could evolve as a single pile throughout its motion and be deposited above or below the bump in the bed; or it could separate in the course of the motion into two piles which are separately deposited above and below the bump.

b) Two-Dimensional

Hutter, Siegel, Savage & Nohguchi [49] added one more dimension to the theory, namely the *cross slope direction*, that is concerned with the motion of an unconfined finite mass of granular material released from rest on an inclined plane. They considered a *free surface flow* of granular material down a slowly varying topography and identified the mean plane surface of this topography with a plane that is parallel to the (x, y)-plane of the three-dimensional Cartesian coordinate system. To explain the model, let the x-coordinate follow the direction of steepest descent, the y-coordinate be parallel to the horizontal lines and the z-coordinate perpendicular to these, see Fig. 3.5. Thus, the z-axis is inclined with respect to the vertical by the angle ζ. The bottom and the free surface of the moving mass will be defined by $z = b\,(x, y, t)$, and $z = s\,(x, y, t)$, respec-

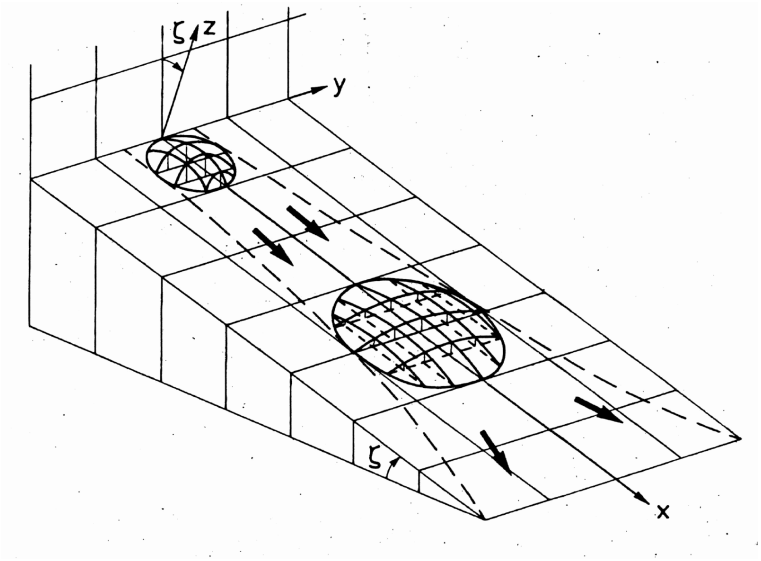

Figure 3.5: Definition of coordinate system and configuration

tively. The depth-averaged equations are deduced from the three-dimensional dynamical equations by scaling the equations and imposing the shallowness assumption that the moving piles are long and wide but not deep. The assumption of confined plane flow conditions is adequate to describe many *flow avalanches*, particularly if they are wide and move on evenly sloped mountain sides. However, avalanches often experience unconfined conditions or are suddenly subject to a relief from a sidewise confinement as will occur when the avalanche moves out of a gorge. In this first analysis of an avalanche with variation of the width of the moving mass, HUTTER et al. [49] reduced the *depth-integrated* equations by performing an additional transversal averaging. This process is performed by assuming a parabolic depth distribution across the width, and longitudinal and transverse velocities which, respectively, have uniform and linear distribution across the width of the pile. A system of spatially one-dimensional partial differential equations in x (the longitudinal variable) and t (time) then yields differential equations for the evolution of the center line depth of the pile, the combined depth- and width-averaged longitudinal velocity components, the distribution of the width of the avalanche and its time rate of change. This model has never been closely followed or explored in any details. It may be of limited use in narrow corrie-flow or free channel flow in industrial applications.

c) Three-Dimensional

GREVE, KOCH & HUTTER [35] presented in detail a three-dimensional extension of the original two-dimensional theory that deals with gravity driven free surface flows of piles of granular materials along bottom profiles that are weakly curved downwards and plane laterally, see Fig. 3.6. The motion is essentially in the direction of steepest descent with small sidewise dispersion. In the laboratory arrangement a pile of granular material held within a hemi-spherical cap (see, e.g., Fig. 10.1) is suddenly released from its rest position and moves down the bed until it comes to rest in the *runout zone*. In this situation a convenient curvilinear coordinate system x, y, z is introduced as follows: x is the downward coordinate fitting the curve profile of the bed that follows the direction of steepest descent; y is the lateral coordinate (in this direction the bed is assumed to be flat); and

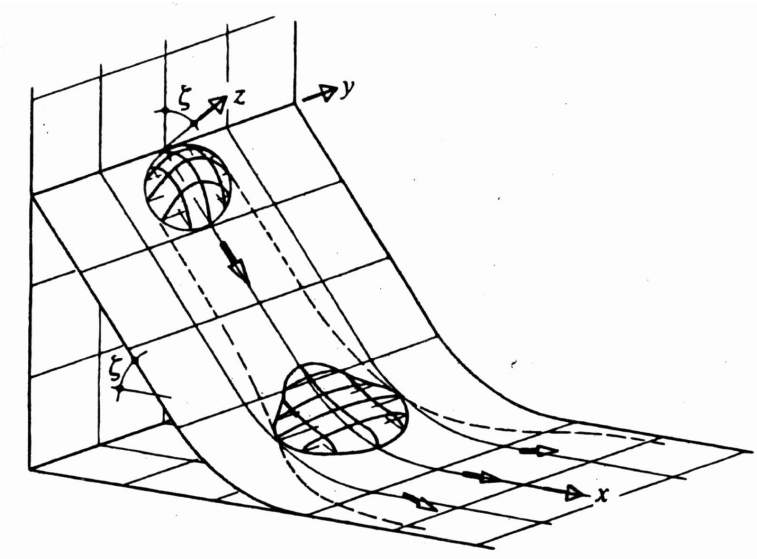

Figure 3.6: Definition sketch of the curvilinear coordinate system fitting the experimental curved surface and geometry of a moving pile of granular material

z is the coordinate perpendicular to the local *tangent plane* of the curved bed as shown in Fig. 3.6.

A further extension of the theory was proposed by Gray, Wieland & Hutter [31]. They presented a two-dimensional depth-integrated theory for the gravity-driven free surface flow of cohesionless granular avalanches, with cross-flow variation of the topography as shown in Fig. 3.7. The *talweg* in this case is still a curve in a vertical plane and has no twist. The situation nevertheless points at an important extension of the one-dimensional SH-theory. In it a simple curvilinear coordinate system is adopted, which is fitted to the mean downslope chute topography. This defines a quasi two-dimensional reference on top of which a shallow three-dimensional basal topography is superposed. We will deal in detail with this extension in the sequel. The reason is that *we can reproduce all of the previous theories as special cases of this model.*

The propagation of *dense flow avalanches* as well as their transition into flows of turbulent particle suspensions in air, i.e., *powder snow avalanches*, has been studied by Zwinger [135] who has modified the Coulomb law for the dry friction with respect to a velocity dependent basal friction law while using the SH-theory for the dense flow part of the avalanche. Comparison between numerical results of the coupled computational model and field data shows generally good agreement [136]. It is, in principle, possible to use this numerical technique for an arbitrarily shaped slope but in the twist free Cartesian coordinates.

Recently, some further advancements of the theory have been achieved. Pudasaini, Eckart & Hutter [99] extended the theory to cases in which curvature and torsion effects of the basal topography are included. In this sense, this is an important extension of the original theory. All the previous extensions were done in a traditional manner as they did not incorporate the *effect of the torsion* of the basal topography through the underlying metric. Natural corries in steep mountainous regions are "meandering"

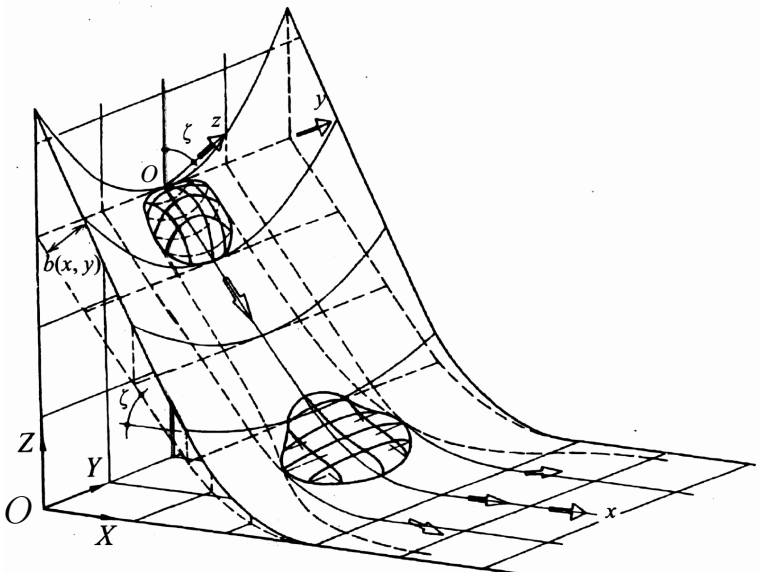

Figure 3.7: The rectangular Cartesian coordinate system $OXYZ$ aligned so that the Z-axis is parallel but opposite in direction to the gravity acceleration vector, and the Y-axis is parallel to the cross-slope reference surface coordinate y. The basal topography (solid lines), on which the avalanche slides, $F^b(\mathbf{x}, t) = 0$, is defined by its height above the curvilinear reference surface $F^b = b(x, y, t) - z$ (dashed lines). The shallow complex three-dimensional geometry is therefore superposed on the two-dimensional curved reference surface

in the landscape which implies that their *talwegs are three-dimensional curves* in three-dimensional space, and these are locally characterised by curvature and torsion (twist). The conceivably most simple situation is a *helical chute*. For such situations it is feasible to base the curvilinear coordinate system on such a three-dimensional master curve. PUDASAINI et al. [99] extended the theory to rapid *shear flows* of dry granular masses in such a rather strongly curved channel having both *curvature* and *torsion*, see later Fig. 5.1. In Chapter 5, we will present a short review on this model.

Quite recently, PUDASAINI & HUTTER [101] extended the theory to a basal topography generated by an *arbitrary space curve having slowly varying curvature and torsion*. Since they can use any space curve to generate the basal topography this extension has many important features as well as enormous applications in real flow situations. In contrast to other previous extensions this local coordinate system is based on a generating line with curvature and torsion. Its derivation was necessary because *real avalanches are often guided by rather curved and twisted corries*. In this way they are able to gain fundamental insight into the effects of *non–uniform curvature and torsion*, using an orthogonal coordinate system that rotates with torsion, and find an analytic description of flow avalanches. This theory is explained in detail in Chapter 4. The major parts of this thesis relay on this theory which *can reproduce all previous extensions of the* SAVAGE-HUTTER*-theory*. In this sense, this theory is very important both from a theoretical as well as application point of view.

3.3 A Three-Dimensional Granular Avalanche Model

In this thesis three variants of extensions of the *SH*-theory will be considered and presented in detail which are applicable to unconfined, confined and curved and twisted avalanche paths with increasing complexity. We present all three because it turns out that they are mathematically very similarly structured and give rise to unified analytical and numerical solution procedures. This recognition is of much help later on when explicit solutions are constructed. The ultimate goal is to present a critical comparison among them and outline their physical meanings and applicabilities in different configurations. The remainder of this Chapter deals with a three-dimensional avalanche model that is associated with an orthogonal curvilinear coordinate system. This model will be referred to as *orthogonal complex system*, complex in the sense that a three-dimensional basal topography that varies both in the longitudinal and lateral direction is superposed on top of a *quasi-two-dimensional* basal reference surface. The other two extensions and generalisations of the *SH*-theory for an *arbitrary reference surface* generated by an orthogonal general coordinate system and a *non-orthogonal helicoidal reference surface* based upon helical coordinates, will be presented in Chapters 4 and 5, respectively.

3.3.1 Field Equations

The avalanche is assumed to be an incompressible, dry and cohesionless material with constant density ϱ_0 throughout the entire body. Then the *mass and momentum conservation laws* reduce to

$$\nabla \cdot \mathbf{u} = 0, \tag{3.1}$$

$$\varrho_0 \left\{ \frac{\partial \mathbf{u}}{\partial t} + \nabla \cdot (\mathbf{u} \otimes \mathbf{u}) \right\} = -\nabla \cdot \mathbf{p} + \varrho_0 \mathbf{g}, \tag{3.2}$$

where ∇ is the gradient operator, $\mathbf{u}$ is the velocity, $\partial/\partial t$ indicates differentiation in time, $\otimes$ is the tensor product, $\mathbf{p}$ is the pressure tensor (the negative CAUCHY stress tensor) and $\mathbf{g}$ is the gravitational acceleration.

The granular avalanche is assumed to satisfy a MOHR-COULOMB *yield criterion* in which the internal shear stress $\mathbf{S}$ and the normal pressure N on any plane element, see Fig. 3.8, are related by

$$|\mathbf{S}| = N \tan \phi, \tag{3.3}$$

where the sign is given by the direction of the sliding velocity and ϕ is the *internal angle of friction*.

The conservation laws (3.1) and (3.2) are complemented by *kinematic boundary conditions* at the free surface, $F^s(\mathbf{x}, t) = 0$, and at the base, $F^b(\mathbf{x}, t) = 0$, of the avalanche

$$F^s(\mathbf{x}, t) = 0, \quad \frac{\partial F^s}{\partial t} + \mathbf{u}^s \cdot \nabla F^s = 0, \tag{3.4}$$

$$F^b(\mathbf{x}, t) = 0, \quad \frac{\partial F^b}{\partial t} + \mathbf{u}^b \cdot \nabla F^b = 0, \tag{3.5}$$

where the superscripts 's' and 'b' indicate that a variable is evaluated at the surface and the base, respectively.

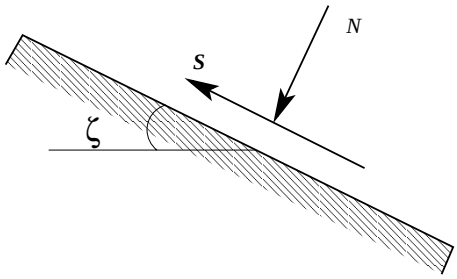

Figure 3.8: Sketch showing the relationship between the internal shear stress **S** and the normal pressure N on a plane element in the granular body

There are also *dynamical boundary conditions* that must be satisfied. The *free surface* of the avalanche is *traction free* while the base satisfies a COULOMB *dry-friction sliding law*:

$$F^s(\mathbf{x},t)=0, \qquad \mathbf{p}^s\mathbf{n}^s=\mathbf{0}, \tag{3.6}$$

$$F^b(\mathbf{x},t)=0, \quad \mathbf{p}^b\mathbf{n}^b-\mathbf{n}^b\left(\mathbf{n}^b\cdot\mathbf{p}^b\mathbf{n}^b\right)=\left(\mathbf{u}^b/|\mathbf{u}^b|\right)\left(\mathbf{n}^b\cdot\mathbf{p}^b\mathbf{n}^b\right)\tan\delta, \tag{3.7}$$

where the surface and basal unit normals are

$$\mathbf{n}^s=\frac{\nabla F^s}{|\nabla F^s|}, \quad \mathbf{n}^b=\frac{\nabla F^b}{|\nabla F^b|}. \tag{3.8}$$

Note: *Notice that* $\mathbf{pn}$ *is the negative traction vector,* $N=\mathbf{n}\cdot\mathbf{pn}$ *is the normal pressure and* $\mathbf{S}=\mathbf{pn}-\mathbf{n}\left(\mathbf{n}\cdot\mathbf{pn}\right)$ *is the negative shear traction. It follows that the* COULOMB *dry-friction law, (3.7), expresses the fact that the magnitude of the basal shear stress equals the normal basal pressure multiplied by a coefficient of friction,* $\tan\delta$*. The parameter* δ *is termed the* basal angle of friction*.*

Note: *Also notice that the shear traction is assumed to point in the opposite direction to the basal velocity* $\mathbf{u}^b$ *in (3.7). This implicitly assumes that* $\mathbf{u}^b\cdot\mathbf{n}^b=0$ *by (3.5). It also implies that the basal velocity* $\mathbf{u}^b$ *is tangential to the basal surface. This then explicitly indicates the condition that the basal surface is independent of time, i.e.,* $\partial F^b/\partial t=0$*. But for the notational convenience we will retain the term* $\partial F^b/\partial t$ *from the field equations wherever they appear.*

Note: *Defining the direction of the shear stress in this way introduces a removable singularity into the equations at* $\mathbf{u}^b=\mathbf{0}$*. This singularity may be avoided by replacing* $\mathbf{u}^b/|\mathbf{u}^b|$ *by the vector valued function*

$$\mathbf{f}_\alpha=\left(f_u,f_v,f_w\right), \tag{3.9}$$

where

$$f_u=\tanh\left(\alpha u\right), \qquad f_v=\tanh\left(\alpha v\right), \qquad f_w=\tanh\left(\alpha w\right), \tag{3.10}$$

in which $\alpha>1$ *is a real number. This parametrisation removes the singularity at* $\mathbf{u}^b=\mathbf{0}$*; moreover, as* $\alpha\to\infty$*,* $\mathbf{f}_\alpha$ *approaches the function* $\mathbf{u}^b/|\mathbf{u}^b|$*. In practical modelling of landslides, rock falls, debris flows and snow and ice avalanches this restriction only causes problems at the onset of the motion and near the end of the avalanche motion, when it seeks to come to rest.*

3.3.2 Curvilinear Coordinate System in a Vertical Plane*

As explained in the previous sections, GRAY et al. [31] extended the SH-theory to model the flow of avalanches over shallow parabolic three-dimensional topography. This led to the first description of the flow of a finite mass of granular material down a valley or corrie. A reference surface that follows the mean downslope bed topography is used to define an orthogonal curvilinear coordinate system, $oxyz$, see Fig. 3.7. The z-axis is normal to the reference surface and the x- and y- coordinates are tangential to it, with the x-axis oriented in the downslope direction. The downslope inclination angle ζ is used to define the reference surface as a function of the downslope coordinate x. *The reference surface does not vary as a function of the cross-slope coordinate* y. The chute geometry is superposed by defining its height $z = b\,(x, y, t)$ above the reference surface, $z = 0$, through the kinematic boundary conditions and the depth integration, as illustrated in Fig. 3.7. Even though the local downslope direction of the basal topography may not coincide with the direction of the x-coordinate, for notational simplicity, the components in the x-direction are referred to as downslope and components in the y-direction as cross-slope components.

Here we will present a brief derivation of the model equations of the theory. For the precise explanation, a rectangular Cartesian coordinate system $OXYZ$ is defined with unit basis vectors $\mathbf{i}, \mathbf{j}, \mathbf{k}$ aligned so that the vector $\mathbf{k}$ is parallel, but in the opposite sense, to the gravity acceleration vector and $\mathbf{i}$ lies in the vertical plane in which the reference surface varies, and $\mathbf{j}$ is perpendicular to both of them. A simple curvilinear coordinate system $oxyz$ is introduced. In this coordinate system, the position vector $\mathbf{r}$ is given by

$$\mathbf{r} = \mathbf{r}^r\,(x, y) + z\mathbf{n}^r, \tag{3.11}$$

where, $\mathbf{r}^r$ is the position vector of the reference surface and $\mathbf{n}^r$ is the normal vector to this surface. In Cartesian coordinates the normal to the reference surface is

$$\mathbf{n}^r = \sin\zeta\mathbf{i} + \cos\zeta\mathbf{k}, \tag{3.12}$$

where, ζ is the inclination angle of the normal of the reference surface relative to the Z-axis. For ease of notation the identification $(x, y, z) = (x^1, x^2, x^3)$ is made. These are the contravariant components in the curvilinear coordinate system (see, e.g., KLINGBEIL [66]), and the associated covariant basis vectors, $\mathbf{g}_i$, are given by

$$\mathbf{g}_i = \frac{\partial \mathbf{r}}{\partial x^i}. \tag{3.13}$$

The gradients $\partial\mathbf{r}/\partial x^1$ and $\partial\mathbf{r}/\partial x^2$ are simply the tangent vectors to the reference surface in the x^1- and x^2-directions, respectively. Thus, choosing the mutually orthogonal tangent vectors with the x-axis in the OXZ plane it follows that $\partial\mathbf{r}^r/\partial x^1 = \cos\zeta\mathbf{i} - \sin\zeta\mathbf{k}$ and $\partial\mathbf{r}^r/\partial x^2 = \mathbf{j}$, so that

$$\begin{aligned} \mathbf{g}_1 &= \left(1 - \kappa x^3\right)\left(\cos\zeta\mathbf{i} - \sin\zeta\mathbf{k}\right), \\ \mathbf{g}_2 &= \mathbf{j}, \\ \mathbf{g}_3 &= \sin\zeta\mathbf{i} + \cos\zeta\mathbf{k}, \end{aligned} \tag{3.14}$$

*In this section and henceforth knowledge of the basic elements of tensor calculus are supposed known. There is a great number of books on this, e.g., BOWEN & WANG, SOKOLNIKOFF, KLINGBEIL, BRILLOUIN [8, 9, 10, 66, 117].

where the curvature κ is given by

$$\kappa = -\frac{\partial \zeta}{\partial x^1}. \tag{3.15}$$

The covariant metric coefficients are defined as $g_{ij} = \mathbf{g}_i \,.\, \mathbf{g}_j$. So, it follows from (3.14) that

$$(g_{ij}) = \begin{pmatrix} (1-\kappa x^3)^2 & 0 & 0 \\ 0 & 1 & 0 \\ 0 & 0 & 1 \end{pmatrix}. \tag{3.16}$$

Since the off-diagonal elements of this metric tensor are all zero, this simple curvilinear coordinate system is called *orthogonal*. The region above the reference surface $z = 0$ can be described by the coordinates xyz that are based on the metric with the square arc length

$$ds^2 = (1-\kappa z)^2\, dx^2 + dy^2 + dz^2. \tag{3.17}$$

The metric is uniquely defined as long as the z-coordinate is locally smaller[†] than $1/\kappa$. In the theory it is assumed to be satisfied automatically. It is clear that (3.17) defines an orthogonal metric.

3.3.3 The Model Equations

A more detailed and explicit derivation of the model equations for a more general case is presented in Chapter 4. Therefore, here we only present a short review of the model equations of Gray et al. [31].

Conservative Form

The coordinate invariant governing equations of Section 3.3.1 are expressed in a first step in the curvilinear coordinate system of Section 3.3.2 as shown in Fig. 3.7. This is done by simultaneously non-dimensionalising the equations via a scaling that introduces an aspect ratio $\varepsilon = \textit{typical height/typical extent}$ and is used to simplify the equations. In a second step, the mass and momentum balance equations are integrated through the avalanche depth along the normal of the reference geometry. In this process terms of order higher than $O(\varepsilon)$ are neglected. For an incompressible cohesionless material the continuity equation yields together with the kinematic boundary conditions at the free surface and the base of the avalanche,

$$\frac{\partial h}{\partial t} + \frac{\partial}{\partial x}(hu) + \frac{\partial}{\partial y}(hv) = 0, \tag{3.18}$$

where h represents the evolving geometry of the avalanche and $\mathbf{u} = (u, v)$ is the depth-averaged surface-parallel velocity with components u and v in the down-slope and cross-slope directions, respectively. Similarly, the momentum balance equations in the down- and cross-slope directions reduce to

[†]Physically these points correspond to the positions at which consecutive z-axes, which vary locally, intersect with one another. Therefore, the superposed topography b, should also be a shallow one. Provided the avalanche does not pass through one of these points during the course of its motion the curvilinear coordinates (3.16) represent a valid coordinate system.

$$\frac{\partial}{\partial t}(hu) + \frac{\partial}{\partial x}\left(hu^2\right) + \frac{\partial}{\partial y}(huv) = hs_x - \frac{\partial}{\partial x}\left(\frac{\beta_x h^2}{2}\right), \tag{3.19}$$

$$\frac{\partial}{\partial t}(hv) + \frac{\partial}{\partial x}(huv) + \frac{\partial}{\partial y}\left(hv^2\right) = hs_y - \frac{\partial}{\partial y}\left(\frac{\beta_y h^2}{2}\right). \tag{3.20}$$

Equations (3.18)–(3.20), which are in *conservative form*, will henceforth be referred to as an *orthogonal complex system*. The factors β_x and β_y are defined as

$$\beta_x = \varepsilon \cos\zeta K_x \quad \text{and} \quad \beta_y = \varepsilon \cos\zeta K_y, \tag{3.21}$$

respectively. The terms s_x and s_y represent the *net driving accelerations* in the down-slope and cross-slope directions, respectively, and are given by

$$s_x = \sin\zeta - \frac{u}{|\mathbf{u}|}\tan\delta\left(\cos\zeta + \lambda\kappa u^2\right) - \varepsilon\cos\zeta\frac{\partial b}{\partial x}, \tag{3.22}$$

$$s_y = \quad - \frac{v}{|\mathbf{u}|}\tan\delta\left(\cos\zeta + \lambda\kappa u^2\right) - \varepsilon\cos\zeta\frac{\partial b}{\partial y}, \tag{3.23}$$

where δ is the *bed friction angle* of the granular material with the basal topography, namely b. K_x and K_y are called the *earth pressure coefficients* which are equal to the ratio of the in-plane to vertical pressure in the down- and cross-slope directions, respectively (that is, $K_x = p_{xx}/p_{zz}$ and $K_y = p_{yy}/p_{zz}$). Elementary geometrical arguments may be used to determine these values as a function of the internal, ϕ, and basal, δ, angles of friction, HUTTER et al. [49]

$$K_{x_{act/pas}} = 2\sec^2\phi\left(1 \mp \sqrt{1 - \cos^2\phi\sec^2\delta}\right) - 1, \tag{3.24}$$

$$K_{y_{act/pas}} = \frac{1}{2}\left(K_x + 1 \mp \sqrt{(K_x - 1)^2 + 4\tan^2\delta}\right), \tag{3.25}$$

where K_x and K_y are *active* during dilatational motion (upper sign) and *passive* during compressional motion (lower sign). The detailed presentation of these statements and computations have been given in Chapter 4, Section 4.7.

The conservation laws (3.18)–(3.20) are written in *non-dimensional curvilinear form*. The non-dimensional variables, $(x, y, h, b, u, v, t, \kappa)$ can be mapped back to their physical counterparts $\left(\hat{x}, \hat{y}, \hat{h}, \hat{b}, \hat{u}, \hat{v}, \hat{t}, \hat{\kappa}\right)$ by applying the scalings

$$(\hat{x}, \hat{y}) = L(x, y), \ \left(\hat{h}, \hat{b}\right) = H(h, b), \ (\hat{u}, \hat{v}) = \sqrt{gL}(u, v), \ \hat{t} = \sqrt{L/g}\,t, \ \hat{\kappa} = \kappa/\mathcal{R}, \tag{3.26}$$

where H is the typical avalanche height, L is the typical avalanche length and $\mathcal{R}$ is a typical radius of curvature of the chute in the down-slope direction, while g is the gravitational acceleration. It is, moreover, assumed that both the aspect ratio $\varepsilon = H/L$ and the characteristic curvature of the chute $\lambda = L/\mathcal{R}$, arising in equations (3.21)–(3.23), are small.

Let us conclude this section with a few words about the physical meaning of the above model equations. The first term on the right-hand side of (3.22) is due to the gravitational acceleration and has no contribution in the lateral, y, direction. The second terms of both equations (3.22) and (3.23) emerge from the dry COULOMB friction and the third terms are associated with the contribution of the basal topography. Equations (3.18)–(3.20) constitute a *two-dimensional conservative system of equations* with source terms. For more detail on the form and the derivation of the conservative equations in compact vectorial structure, we refer to Section 4.9.3.

Non-Conservative Form

For *smooth solutions* the mass balance (3.18) can be used to simplify the convective terms in the momentum equations (3.19) and (3.20). With

$$\frac{d}{dt} = \frac{\partial}{\partial t} + u\frac{\partial}{\partial x} + v\frac{\partial}{\partial y}, \tag{3.27}$$

the conservative equations change into the following non-conservative form:

$$\frac{du}{dt} = \sin\zeta - \frac{u}{|\mathbf{u}|}\tan\delta\left(\cos\zeta + \lambda\kappa u^2\right) - \varepsilon\cos\zeta\left(K_x\frac{\partial h}{\partial x} + \frac{\partial b}{\partial x}\right), \tag{3.28}$$

$$\frac{dv}{dt} = -\frac{v}{|\mathbf{u}|}\tan\delta\left(\cos\zeta + \lambda\kappa u^2\right) - \varepsilon\cos\zeta\left(K_y\frac{\partial h}{\partial y} + \frac{\partial b}{\partial y}\right), \tag{3.29}$$

provided that $h \neq 0$. The system of equations (3.18), (3.28) and (3.29) constitute a *non-conservative system of equations*, derived originally by GRAY et al. [31] to generalise the one-dimensional SH-theory [112, 113]. The non-conservative form is useful to implement the LAGRANGIAN numerical scheme, for more detail see [31, 121, 131].

Given the reference surface (slope) $\zeta(x)$, a basal topography $b(x, y, t)$ and the material slip parameters δ and ϕ, both of these systems of equations allow three independent variables h, u and v to be computed once the initial conditions and boundary conditions at the edge of the avalanche domain are prescribed.

Now, we are in a position to formulate the SAVAGE-HUTTER continuum mechanical theorem for dense granular avalanches in a "compact and precise mathematical form". The theory is based on a *hydraulic* framework and generalises the *mass point model* of VOELLMY [127].

Theorem: Savage-Hutter Avalanche Theorem

We consider the following assumptions:

(i) Topography: *A reference surface can be described by an orthogonal curvilinear coordinate system $\mathcal{O}xyz$ in which the z-axis is normal to the surface and the x- and y-axes are tangential to it, with the x-axis oriented downslope. The function $\zeta = \zeta(x)$ represents the downslope inclination to the horizontal and $\kappa = -\partial\zeta/\partial x$ is its curvature. Suppose $z = b(x, y, t)$ is the chute geometry above this surface and $z = s(x, y, t)$ the free surface so that $h(x, y, t) = s(x, y, t) - b(x, y, t)$ represents the avalanche height along the z-axis.*

(ii) Material: *The avalanche is assumed to consist of a shallow, incompressible, non-cohesive, isothermal, stress-symmetric, dry and dense continuum material.*

(iii) Closure: *Assume that the material satisfies the* COULOMB*-dry friction law at the slide and the* MOHR-COULOMB *plastic yield in the interior, and the dominant deformation takes place in the downslope direction. The shear stresses lateral to the main flow direction can be neglected. Furthermore, the downslope and cross-slope pressures vary linearly with the normal pressure through the depth of the avalanche, and shearing takes place in a very small basal layer so that the velocity distribution is almost uniform over the depth.*

(iv) Pressure Coefficients and Parameters: *Let δ and ϕ be the bed and internal friction angles, respectively, of the granular material and let the pressure coefficients $K_{x,y} = K_{x,y}(\delta, \phi)$ be functions constructed by using the* MOHR *circle with respect to the closure property of the form*

$$K_x = 2\sec^2\phi\left\{1 \mp \left(1 - \cos^2\phi\sec^2\delta\right)^{1/2}\right\} - 1, \tag{3.30}$$

$$K_y = \frac{1}{2}\left\{K_x + 1 \mp \left((K_x - 1)^2 + 4\tan^2\delta\right)^{1/2}\right\}, \tag{3.31}$$

at the bed for the extension and contraction of the material body. Let, moreover, H, L and $\mathcal{R} = 1/\kappa$ be a typical avalanche thickness and length, and the radius of curvature. Define, $\varepsilon = H/L$, $\lambda = L/\mathcal{R}$, and

$$\beta_x = \varepsilon\cos\zeta K_x, \qquad \beta_y = \varepsilon\cos\zeta K_y, \tag{3.32}$$

$$s_x = \sin\zeta - \frac{u}{|\mathbf{u}|}\tan\delta\left(\cos\zeta + \lambda\kappa u^2\right) - \varepsilon\cos\zeta\frac{\partial b}{\partial x}, \tag{3.33}$$

$$s_y = \quad - \frac{v}{|\mathbf{u}|}\tan\delta\left(\cos\zeta + \lambda\kappa u^2\right) - \varepsilon\cos\zeta\frac{\partial b}{\partial y}, \tag{3.34}$$

where $\mathbf{u} = (u, v)$ is the depth-averaged surface-parallel velocity with components u and v along the x- and y-coordinates, respectively.

(v) Smoothness: *Suppose that all field variables are sufficiently smooth to change the order of integration and differentiation.*

Then, under a realistic non-dimensionalisation, the dynamics of a granular avalanche can be described by the following set of partial differential equations

$$\frac{\partial h}{\partial t} + \frac{\partial}{\partial x}(hu) + \frac{\partial}{\partial y}(hv) = 0, \tag{3.35}$$

$$\frac{\partial}{\partial t}(hu) + \frac{\partial}{\partial x}\left(hu^2\right) + \frac{\partial}{\partial y}(huv) = hs_x - \frac{\partial}{\partial x}\left(\frac{\beta_x h^2}{2}\right), \tag{3.36}$$

$$\frac{\partial}{\partial t}(hv) + \frac{\partial}{\partial x}(huv) + \frac{\partial}{\partial y}\left(hv^2\right) = hs_y - \frac{\partial}{\partial y}\left(\frac{\beta_y h^2}{2}\right), \tag{3.37}$$

accurate to order $\varepsilon^{1+\gamma}$, $0 < \gamma < 1$.

Note: *The physical variables are recovered by realistic non-dimensionalisations as pointed out by equation (3.26).*

3.3.4 Distinguished Features and Limitations of the SH-Theory

There are many distinguished advantageous features of the SH-theory. Needless to say, there are some limitations too. We point out them systematically as follows:

Advantages:

- *A Complete Theory:* The SH-model equations provide a complete dynamic description of the avalanche, debris flow or small scale industrial flows in channels, hoppers, silos or heap formations from initiation via its path to the run-out or still stand and deposition. The dynamics of any avalanche is associated to the evolution of the avalanche geometry and the velocity distribution over the entire body. Consequently, one can easily predict the impact pressure on obstructions along the way of the avalanche or the debris. The main intention of the SH-model is to provide these properties of the flowing geo- and industrial granular-masses.

- *A Three-Dimensional Mapping:* There is no other avalanche model[‡] which can provide a three-dimensional avalanche mapping along its path to the run-out. There are some mass-point and statistical models (as explained earlier in Section 2.6) which can only provide a means of one-dimensional mapping. The SH-model provides the required three-dimensional mappings sought by the avalanche practitioners and civil engineers to separate a mountain valley into "red, yellow and green" regions in order to protect the life and property of the valley inhabitant.

- *Scale Invariant:* The SH-model equations are scale invariant. Since the model equations are non-dimensionalised, they can be used from a very small (several cubic centimeters) laboratory motions upto very huge (several thousand million cubic meters) natural catastrophes.

- *Slope Fitted Model Equations:* The SH-model equations are derived in natural slope fitted coordinates that are compatible with the real bed over which the avalanche moves. Consequently, this model can capture the effects of topographic curvature. None of the other existing models possesses this property.

- *Handy and Economical:* The SH-model is very simple to implement in the sense that one needs to know only two physical parameters: the internal angle of friction and the bed friction angle, and the flow topography. In most cases, the material or the phenomenological parameters can be determined in the laboratory and the basal surface can be constructed from remote digital altimeter data. What is most needed is the initial geometry at the time of the trigger and the initial velocity (usually zero). In the laboratory this is absolutely no problem and in the field it can be determined from the deposited mass, material property, the slope structure and the conservation of the mass. One does not face any larger difficulties with a complicated boundary value problem as in the case when using the kinetic theory or with big super computers with parallel computing as in the molecular dynamics and discrete element models. The SH-model equations can numerically be solved very quickly, in the order of magnitude of few minutes.

[‡]Exceptions are NAVIES-STOKES-models, but they are physically inadequate.

- *Mathematically well Structured:* The model equations of SAVAGE & HUTTER can be brought into the standard form of two-dimensional non-linear hyperbolic partial differential equations with source terms. Very robust numerical solution schemes have been and are still being successfully developed to solve these equations, from the classical finite difference to modern finite element schemes. Moreover, shock capturing and front tracking total variation diminishing numerical schemes are being implemented for these equations in order to capture possible shocks. We will develop and implement such numerical schemes in Chapters 6, 7, 8 and 10.

- *Possibility of Validation by Laboratory Experiments:* The model equations can easily be validated by well-controlled laboratory experiments of confined as well as non-confined avalanche motions of different granular materials. Previous experiences have demonstrated good to excellent correlations between the theoretical predictions and the laboratory simulations via the numerical computations. Even when the theory is compared with field data (of natural hazards), the result is quite good. This makes the theory more reliable in diverse applications. Other classical avalanche models do not possess these important features.

- *Reduction to the Shallow Water Equations:* As a special case, the model equations of SAVAGE & HUTTER reduce to the classical sallow water equations. For this, one needs only to set the earth pressure coefficients to unity, because fluids, like water, do not extend or contract as they pass through a topography with variable curvature. Also these model equations can be used to model actual river dynamics as they include the real topography of the river bed.

- *Extension to Complicated Mountain Topography:* One of the most important features of the SH-model is that it can be extended to describe the real flow of an avalanche and debris in natural and complicated mountain terrain. We will make this fact clear in Chapter 4 by developing a new theory that can predict such flows.

Limitations:

- *Parameters:* The theory holds true only if the internal friction angle is greater than or equal to the bed friction angle. In most engineering and geophysical flows this restriction is not a problem. But, otherwise the theory fails.

- *Geometry:* The theory gives good to excellent results if the topography varies gently. One may not expect good results if there are abrupt changes in the topography in a large sub-region of the flow path. Also, the avalanching body should not exceed, in its height, the radius of curvature and not pass through the center of the curvature of the basal topography.

- *Flow Rules:* There are two opinions about the dry COULOMB friction law implemented in the SH-theory. ANCEY & MEUNIER [3], recently implemented field data of different avalanches in order to infer the bulk frictional forces on the basis of the knowledge of the velocity variation and the depth profiles of the events. They concluded that the COULOMB friction model can be used to describe variations in velocity and frictional forces during the course of an avalanche. While on the other hand, some people argue that it would be better to include the viscous contribution to the basal drag [21, 93, 94]. To some extent this is correct. However, its

incorporation is trivial, but not necessary for cohesionless granular materials. The incorporation of this viscous drag has not been convincingly demonstrated for such restricted applications. For snow avalanches it will be necessary, and when real computations are performed, this viscous drag can be incorporated [135, 136].

In the model, it is assumed that the velocity profile varies uniformly through the depth of the avalanche. Actually, a closure would be needed to include other possibilities which would produce a lot of parameters for all averaged product quantities. But it is very difficult to identify all these parameters.

In the derivation of the model equations, it is assumed that the lateral confinement pressure is close to a principal stress. It is an "ad-hoc" criterion. Incidentally, this assumption is justified whenever lateral velocities and their variations are small as compared to "downhill" velocities.

- *Incompressibility:* The model equations are designed to describe the overall dynamics of the avalanche. But locally, in the starting region, while approaching the deposition zone and in the vicinity of obstructions on the way of the avalanche, the prediction of the model may not be as good as in other parts of the channel. This is due to the large (relative) dilatation of the body in these critical zones.

- *Combination of the First and Leading Orders:* The final governing equations involve terms of $O(1)$ and $O(\varepsilon)$, which is standard in the SH-theory. No other techniques, like a different scaling or a formal perturbation expansion, have so far been found that yield only $O(1)$ terms in the final equations.

In Chapter 4, we will generalise this theory so as to study the dynamics of avalanches, debris-, mud-flows, landslides and rockslides over a non-trivial mountain topography which might be arbitrarily curved and twisted.

Chapter 4

Rapid Shear Flows of Dry Granular Masses in Arbitrarily Curved and Twisted Channels

4.1 Motivation

The model equations presented by HUTTER and coworkers [31, 112, 113] were derived with the intention to be able to describe the motion of a finite mass of granular material down a mountain side into a deposition area. The underlined curvilinear coordinate system was based on a so-called *ruled surface** of which the generating base curve was in a vertical plane, and the ruled straight lines would be kept parallel to one another, whilst the third coordinate would be perpendicular to these, see Fig. 4.1. The topographies permissible for this special coordinate system would be small deviations from the reference surface $b = b(x, y, t)$. Whereas this allows for a large variety of topographies to be studied, see Chapter 3, *the geometries are* nevertheless *restricted*. For instance, the motion in a rather strongly curved channel having both curvature and torsion cannot be analysed with the mentioned curvilinear coordinate system. Such cases do, however, realistically occur. In the transportation of solid materials a finite mass of a dry granular material may have to be transported through a curved and twisted channel (e.g., with helicoidal surface, we refer to Fig. 5.1a). Similarly, the flow of snow or debris avalanches down a mountain corrie may be treated as a flow through a channel, of which the talweg is any prescribed three-dimensional curve with curvature and torsion in the physical space, see Figs. 4.2 and 4.3. Both situations give rise to alternative formulations in settings with their own coordinate system.

In this chapter we present a review of a recent two-dimensional depth-integrated theory developed by PUDASAINI & HUTTER [101] for the gravity-driven free surface flow of a granular avalanche over an arbitrarily but gently curved and twisted topography which

*A ruled surface is a surface which can be swept out by a moving line in space and therefore has a parameterisation (with parameters u and v) of the form

$$R(u, v) = b(u) + vd(u),$$

where b is called the *base curve* (also called the *directrix*) and d is the *director curve*. The straight lines themselves are called *rulings*. The rulings of a ruled surface are *asymptotic curves*.

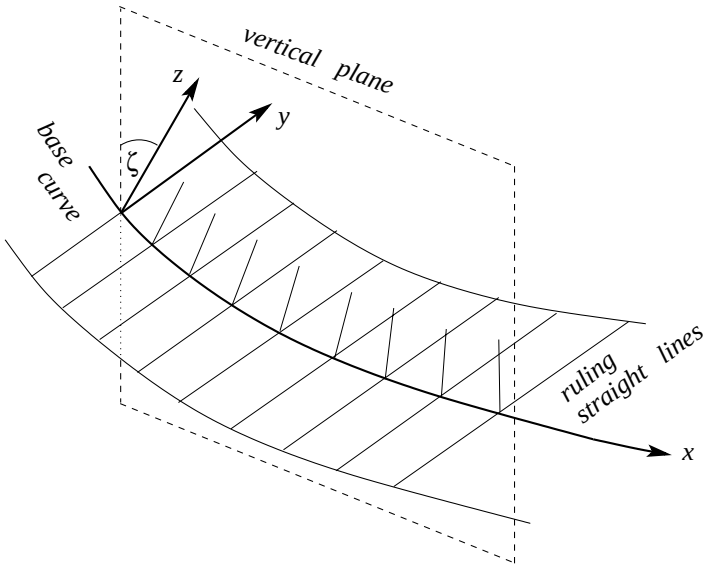

Figure 4.1: Ruled surface, constructed from a generating base curve in a vertical plane and parallel ruling straight lines. The three families of curves define the curvilinear coordinate system x, y, z

is a very important extension of the original SH-theory. In contrast to other previous extensions this local coordinate system is *based on a generating line with curvature and torsion*. The theory is based on an orthogonal metric, associated with curvature and torsion of a basal topography that is generated by an arbitrary three-dimensional curve in physical space. It allows relatively easy access to comparison with laboratory experiments as well as field events. The aim of the theory is to gain fundamental insight into the *effects of non–uniform curvature and torsion*, using an orthogonal coordinate system that rotates with curvature and torsion, and to find an analytic description of flow avalanches. As before, PUDASAINI & HUTTER [101] assume a shallow avalanche of a dry cohesionless granular material, incompressible with constant density ρ_0 throughout the motion from initiation to the run-out zone. The motion follows the talweg of a curved and twisted channel. Balance laws of mass and momentum, kinematic boundary conditions on the basal and free surface, the COULOMB–dry friction law at the base and the tractionless free surface condition constitute the underlying *moving boundary value problem*. Depth averaging the field equations leads to a set of non–linear partial differential equations for the space and time evolution of the granular pile height and the depth-averaged streamwise velocity distribution of a finite mass of granulates. COULOMB–like constitutive behaviour both for the bed and interior of the granular body is employed. An enormous and significant simplification is achieved by the depth averaging process.

The emerging theory is a generalisation of the successful SH avalanche model and is capable of predicting the flow of dense granular materials over moderately curved and twisted channels of general type. The derivation of this new theory starts from a quite different geometrical and analytical setting. But, surprisingly enough, the present theory can exactly reproduce all previous model equations of the SH-theory. The model equations are tested and validated by numerical simulations as well as controlled laboratory avalanches of dry and cohesionless finite mass of different granulates which have similar properties to those of natural avalanches and debris. This will be dealt with in detail in Chapters $6 - 10$.

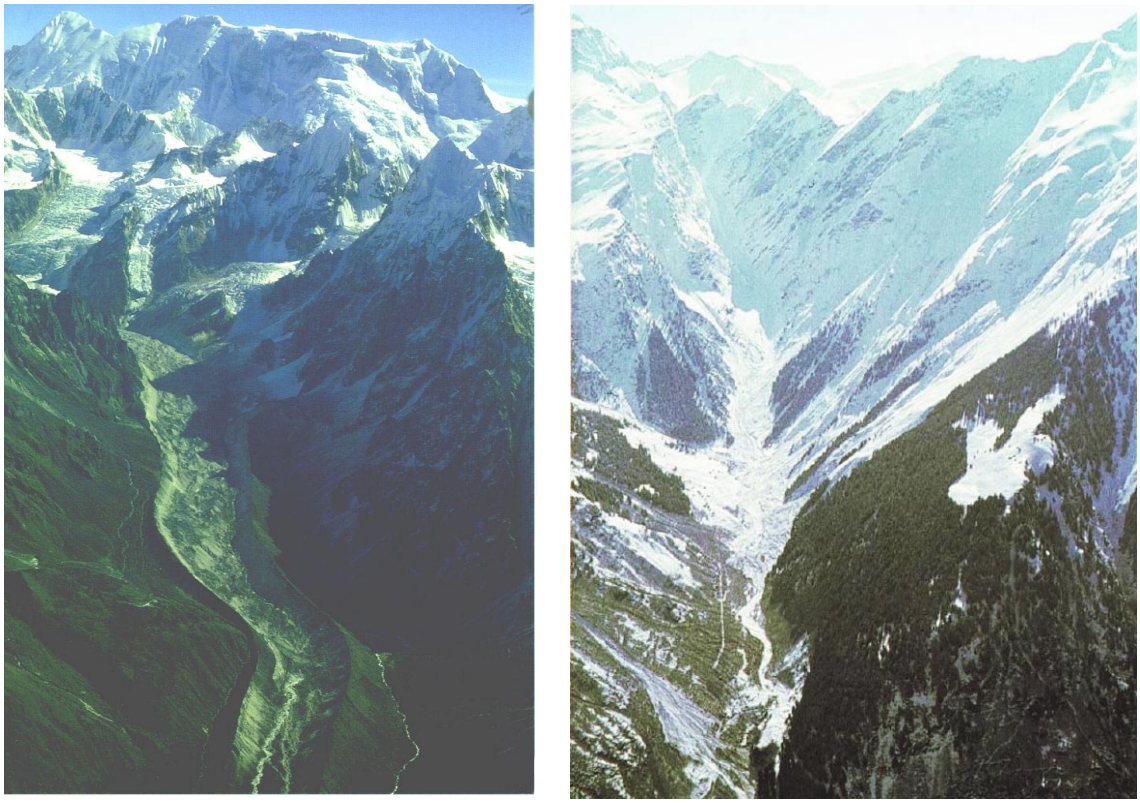

Figure 4.2: Examples of curved and twisted natural corries in geophysical scenarios. In both pictures, the talweg of the valley can easily be identified as a smooth three-dimensional space curve

4.2 The Essence of the New Theory

As mentioned, Pudasaini & Hutter [101] extended the SH-theory to rapid shear flows of dry granular masses in a *non–uniformly curved and twisted channel* having both *curvature and torsion*. In the study of the flow of an avalanche in a channel whose *axial line*, (henceforth called the "master curve" or the "reference curve") is a *generic spatial line* it is important to choose an appropriate system of coordinates. In this theory one may assume that the curvature and torsion of the master curve are known as functions of the arc length s, $\kappa = \kappa(s), \tau = \tau(s)$. Then, an orthogonal coordinate system along the generic master curve can be introduced (see, e.g., Germano and Zabielski & Mestel [27, 28, 133, 134]) and the SH-equations for a non–steady, incompressible, dry and cohessionless granular avalanche explicitly derived in this frame of reference. We thus studied in [101] the simultaneous effects of curvature and torsion on the flow avalanche in channels which could not be investigated before.

This theory is aiming to provide evidence that the SH-theory works well also for topographies having curvature and torsion. This makes the present model *amenable to realistic avalanche motions down arbitrarily guided topographies* such as valleys and channelised corries. In fact, *Geographic Information Systems* (GIS) applied to mountainous avalanche-prone regions can be applied to this model. It provides the analytical and geometrical basis for an application close to realistic situations and tuned to practical use. This chapter lays the theoretical foundation towards this end. Different from the

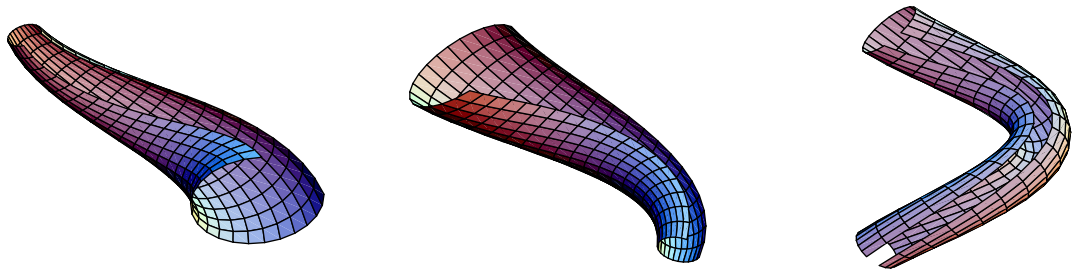

Figure 4.3: Diverging, converging and uniform curved and twisted channels that can be used in the transportation of the granular materials

original SH-theory [112, 113], we choose an arbitrary space curve and use it to define an orthogonal–curvilinear coordinate system. As in the SH-model, we formulate the balance laws of mass and momentum as well as the boundary conditions in terms of these coordinates, average these equations over depth and then non-dimensionalise the averaged equations. There is, however, a subtle difference in non-dimensionalising the equations and in the ordering analysis as compared to the original theory. The final governing balance laws of mass and momentum appear to be much less complicated with the averaging operation performed due to the use of an orthogonal basis constructed in a special way.

In what follows we will present this theory in detail. The derivation of the field equations in their coordinate free form can be taken over from Section 3.3.1. Here we will just refer to those equations whenever they are explicitely needed. Therefore, we will start the analysis of the flow by presenting the underlying curvilinear coordinate system.

4.3 General Orthogonal Coordinate System

Consider an avalanche-prone landscape and a subregion of it where the topography allows the identification of an avalanche track, see Fig. 4.2. A curve, following the landscape topography (e.g., the talweg of the valley) is singled out as a master curve C from which the track topography will be modelled. Let this three–dimensional curve be smooth; in the global coordinate system it may be given by $\mathbf{R}(x, y, z)$, where x, y and z are the Cartesian coordinates. A moving coordinate system is constructed (see, e.g., Klingbeil, Bowen & Wang, Germano, Zabielski & Mestel, [8, 9, 27, 28, 66, 133, 134]) by considering this spatial curve described by the position vector $\mathbf{R}(s)$, where s is the parameter that measures the arc length from some convenient reference point. At any point of the curve we have the orthonormal triad $\{\mathbf{T}, \mathbf{N}, \mathbf{B}\}$ which, respectively, comprises of the tangent, principal normal and binormal unit vectors, also expressible as functions of s. The vector pair $\{\mathbf{N}, \mathbf{B}\}$ spans a plane perpendicular to C. Any Cartesian vector $\mathbf{X}$ in the three-dimensional space can be expressed as

$$\mathbf{X} := \mathbf{X}(s, r, \theta) = \mathbf{R}(s) + r\cos\left(\theta + \varphi(s) + \varphi_0\right)\mathbf{N}(s) + r\sin\left(\theta + \varphi(s) + \varphi_0\right)\mathbf{B}(s). \qquad (4.1)$$

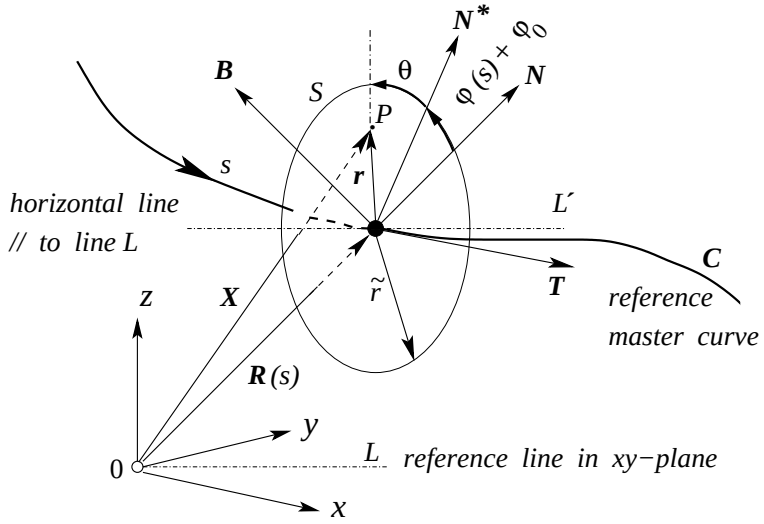

Figure 4.4: A sketch and description of a moving coordinate system and generation of a mountain corrie: $\mathbf{R}(s)$ describes the reference (master) curve C embedded in $\mathbb{R}^3$. s is the arc length, $\{\mathbf{T}, \mathbf{N}, \mathbf{B}\}$ is the moving orthonormal unit triad following the curve. (r, θ) are polar coordinates spanning the plane of circle S with radius $\tilde{r}$ normal to the axis of C. The origin of the azimuthal angle, θ, in this plane is arbitrary, but measured from the unit vector $\mathbf{N}^*$ which is rotated from $\mathbf{N}$ by a phase $(\varphi(s) + \varphi_0)$ for an $s \in [s_0, \infty)$, $s_0 \in [0, \infty)$ and $\theta \in (0,\, 2\pi]$. Also φ_0 is an arbitrary constant and P is any point in space

Here, (r, θ) are polar coordinates spanning the plane normal to the axis of the master curve C in Fig. 4.4, and s is the arc length[†]. The origin of the azimuthal angle, θ, in this plane is arbitrary, but measured from the unit vector $\mathbf{N}^*$ which is rotated from $\mathbf{N}$ by *a phase* $(\varphi(s) + \varphi_0)$. Also φ_0 is an arbitrary constant (in applications often conveniently taken as 0 or $\pm\pi/2$) and

$$\varphi(s) = -\int_{s_0}^{s} \tau(s')ds' \tag{4.2}$$

is the *accumulation of the torsion* of the curve as it proceeds from the initial point s_0. Hence the torsion, $\tau(s)$, enters into the equations through the auxiliary function $\varphi = \varphi(s)$. From Differential Geometry (see, Bowen & Wang and Klingbeil [8, 9, 66]) we recall the following results:

$$\mathbf{T}(s) = \frac{d\mathbf{R}(s)}{ds}, \quad \mathbf{N}(s) = \frac{1}{\kappa(s)}\frac{d\mathbf{T}(s)}{ds}, \quad \mathbf{B}(s) = \mathbf{T}(s) \times \mathbf{N}(s), \tag{4.3}$$

where $\kappa(s)$ is the curvature of the master (reference) curve C and "$\times$" stands for the "cross product" of two vectors. Curvature and torsion can be computed from the function $\mathbf{R} = \mathbf{R}(x, y, z)$ and are intrinsically expressible as functions of the arc length s: $\kappa = \kappa(s)$

[†]We have assumed here that the arc length is either known or can be computed. If t is another parameterisation of the reference curve then

$$s = \int_{t_0}^{t} |\dot{R}(t')|dt',$$

where t_0 is the parameter value for which $s = 0$.

and $\tau = \tau(s)$. The famous SERRET–FRÉNET formulas provide a connection between the curvature and torsion and the changes of $\mathbf{T}, \mathbf{N}, \mathbf{B}$ along s as follows:

$$\frac{d\mathbf{T}}{ds} = \kappa\mathbf{N}, \quad \frac{d\mathbf{N}}{ds} = \tau\mathbf{B} - \kappa\mathbf{T}, \quad \frac{d\mathbf{B}}{ds} = -\tau\mathbf{N}. \tag{4.4}$$

One can easily show that the metric for the chosen coordinate system is given by

$$d\mathbf{X} \cdot d\mathbf{X} = \left[1 - \kappa(s) r \cos\left(\theta + \varphi(s) + \varphi_0\right)\right]^2 (ds)^2 + (dr)^2 + (r d\theta)^2 . \tag{4.5}$$

This corroborates orthogonality of the system (4.1) and (4.3). It is also easy to see that when $\tau = 0$ this system of coordinates reduces to the simple toroidal, while it reduces to the cylindrical coordinate system when $\kappa = \tau = 0$.

This system of coordinates is well known to researchers involved in studies on hydromagnetic equilibria. It was first introduced by MERCIER [84], and was extensively used by SOLOVE'V & SHAFRANOV [118] in their computations of plasma confinement in closed magnetic systems. GERMANO [27] wrote the NAVIER–STOKES equations for an incompressible viscous fluid in these coordinates; and GERMANO [28] extended the DEAN equations [14, 15] to the case of a helical pipe flow in this orthogonal system of coordinates. Recently, GAMMACK & HYDON [26] studied steady and unsteady flows in pipes with small, slowly varying curvature and torsion using GERMANO's extension of the DEAN equations. PUDASAINI & HUTTER [101] also utilised this special coordinate system in order to investigate the dynamics of the *gravity driven* rapid shear flow of *large scale geomaterials* down curved and twisted channels.

Because *Geographical Information Systems* (GIS) refer the topography to the global Cartesian system $\{x, y, z\}$ this must in a particular application first be transformed to the orthogonal moving coordinate system. This can be done and is generally done by NURBS (Non–Uniform Rational B–Spline), see PIEGL & TILLER [89]. It will in this Chapter not be of any concern because our focus will be on the derivation of the model equations for an arbitrary topography. The most advantageous fact of this moving coordinate system along a curved and twisted line is that we are free to choose the *master curve*. Hence it may have enormous applications in investigations of the flow behaviour of fluids as well as moving granular materials in a curved and twisted channel.

For ease of notation the identifications

$$(x^1,\, x^2,\, x^3) = (s,\, \theta,\, r) \tag{4.6}$$

will be made.

The tangent vectors to the coordinate lines, i.e., the associated covariant basis vectors, $\mathbf{g}_i = \partial\mathbf{X}/\partial x^i$ (see Fig. 4.5), are given by

$$\begin{aligned} \mathbf{g}_1 &= (1 - \kappa r\eta)\, \mathbf{T}(s), \\ \mathbf{g}_2 &= -r\zeta\mathbf{N}(s) + r\eta\mathbf{B}(s), \\ \mathbf{g}_3 &= \eta\mathbf{N}(s) + \zeta\mathbf{B}(s), \end{aligned} \tag{4.7}$$

where

$$\eta = \cos\left(\theta + \varphi(s) + \varphi_0\right), \qquad \zeta = \sin\left(\theta + \varphi(s) + \varphi_0\right). \tag{4.8}$$

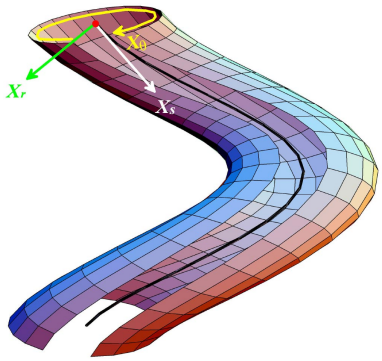

Figure 4.5: A representation of a curved and twisted channel, a reference curve and the tangent vectors along the coordinate lines. The dark line along the channel is the axis of the channel

The covariant metric, defined as $(g_{ij}) = (\mathbf{g}_i \,.\, \mathbf{g}_j)$, and the associated contravariant metric $(g^{ij}) = (g_{ij})^{-1}$, turn out to be

$$(g_{ij}) = \begin{pmatrix} (1-\kappa r\eta)^2 & 0 & 0 \\ 0 & r^2 & 0 \\ 0 & 0 & 1 \end{pmatrix}, \quad (g^{ij}) = \begin{pmatrix} 1/(1-\kappa r\eta)^2 & 0 & 0 \\ 0 & 1/r^2 & 0 \\ 0 & 0 & 1 \end{pmatrix}. \tag{4.9}$$

The covariant unit vectors are defined as $\mathbf{g}_i^* = \mathbf{g}_i/\sqrt{g_{(ii)}}$. It is clear that in contrast to the standard Cartesian unit vectors $\mathbf{i}, \mathbf{j}, \mathbf{k}$, the covariant vectors $\mathbf{g}_i$ vary as functions of position.

The Christoffel symbols of second kind[‡] are needed to express the differential operators grad and div in order to transfer the equations of motion from the coordinate free form to the curvilinear coordinates. This is a standard method when tackling geophysical flow processes with complicated boundary and topographic conditions. In an orthogonal coordinate system, they are defined as (see, e.g., Bowen & Wang and Klingbeil, [8, 9, 66])

$$\Gamma^k_{lm} = \tfrac{1}{2} g^{(kk)} \left(g_{mk,l} + g_{kl,m} - g_{lm,k}\right), \tag{4.10}$$

in which the Einstein summation convention is dropped for the bracketed indices. For the curvilinear coordinates (4.9) the components of the Christoffel symbol are

$$\mathbf{\Gamma}^1 = -\psi \begin{pmatrix} \Lambda r & -\kappa r\zeta & \kappa\eta \\ -\kappa r\zeta & 0 & 0 \\ \kappa\eta & 0 & 0 \end{pmatrix}, \mathbf{\Gamma}^2 = \frac{1}{r} \begin{pmatrix} -\kappa\zeta/\psi & 0 & 0 \\ 0 & 0 & 1 \\ 0 & 1 & 0 \end{pmatrix}, \mathbf{\Gamma}^3 = \begin{pmatrix} \kappa\eta/\psi & 0 & 0 \\ 0 & -r & 0 \\ 0 & 0 & 0 \end{pmatrix}, \tag{4.11}$$

where

$$\Lambda = \kappa'\eta + \kappa\tau\zeta, \quad \psi = 1/(1-\kappa r\eta) \quad \text{and} \quad \kappa' = \partial\kappa/\partial s. \tag{4.12}$$

Further, the vector differential operator ∇ is defined as

$$\nabla = \mathbf{g}^k \frac{\partial}{\partial x^k}, \tag{4.13}$$

[‡]The Christoffel symbols of second kind are defined as $\Gamma^k_{ij} = \left(\partial \mathbf{g}_i/\partial x^j\right) \cdot \mathbf{g}^k$.

with components given in terms of the contravariant basis $\mathbf{g}^k$; and the gradient of a given scalar field F is $\nabla F = F_{,k}\,\mathbf{g}^k$. For the curvilinear coordinate system defined in (4.9), in terms of the covariant unit basis, this can be expressed as

$$\nabla F = \psi\frac{\partial F}{\partial s}\mathbf{g}_1^* + \frac{1}{r}\frac{\partial F}{\partial \theta}\mathbf{g}_2^* + \frac{\partial F}{\partial r}\mathbf{g}_3^*. \tag{4.14}$$

The prefactors of $\mathbf{g}_j^*$ are called the *physical components* of the gradient of F.

The divergence of a vector field $\mathbf{u} = u^i\mathbf{g}_i$ and a symmetric second–order pressure tensor $\mathbf{p} = p^{ij}\mathbf{g}_i \otimes \mathbf{g}_j$, respectively, are expressed as

$$\nabla\cdot\mathbf{u} = \left(\mathbf{g}^k\frac{\partial}{\partial x^k}\right)\cdot\left(u^i\mathbf{g}_i\right) = u^i_{,\,i} + u^i\Gamma^k_{ik}, \quad \Gamma^k_{ik} = \mathbf{g}^k\cdot\mathbf{g}_{i,k}, \tag{4.15}$$

$$\nabla\cdot\mathbf{p} = \left(\mathbf{g}^k\frac{\partial}{\partial x^k}\right)\cdot\left(p^{ij}\mathbf{g}_i\otimes\mathbf{g}_j\right) = \{p^{ki}{}_{,\,k} + p^{ji}\Gamma^k_{jk} + p^{kj}\Gamma^i_{jk}\}\sqrt{g_{(ii)}}\mathbf{g}_i^*. \tag{4.16}$$

For notational brevity and to make the present theory compatible with previous model equations of the SH-theory, we define the following new variables:

$$(x, y, z) := (s, r\theta, r). \tag{4.17}$$

From now on all derivations are done with respect to these new variables: First we take the differentials with respect to these variables and then we again shift the z coordinate by an amount z_T, i.e., we replace z by $z + z_T$, where z_T is the distance between the master curve and the talweg, see Fig. 4.10. Therefore, (x, y, z) are, from now on, *not* Cartesian components, but rather the coordinates of the curved and twisted channel, and the origin of this new coordinate system lies in the talweg. Furthermore, the manifold $z = const.$ forms a curved reference surface and the new variable z is the coordinate in the direction normal to it. We refer to the $x, y,$ and z coordinates as downslope, cross–slope and normal directions, respectively. In the following computations we write

$$\mathcal{Z} = z + z_T. \tag{4.18}$$

The physical components of the vector $\mathbf{u}$ are defined by $u^{i*} = u^i\sqrt{g_{(ii)}}$. Similarly, the physical components p^{ij*} of a second order tensor $\mathbf{p}$ are related to the contravariant components by $p^{ij*} = p^{ij}\left(\sqrt{g_{(ii)}}\sqrt{g_{(jj)}}\right)$. With these physical components together with the Christoffel symbols (4.11), expressions (4.15) and (4.16), in curvilinear coordinates, respectively, read

$$\nabla\cdot\mathbf{u} = \frac{\partial}{\partial x}\left(\psi u^{1*}\right) + \frac{\partial u^{2*}}{\partial y} + \frac{\partial u^{3*}}{\partial z} - \psi^2\Lambda\mathcal{Z}u^{1*} + \psi\kappa\zeta u^{2*} - \left(\psi\kappa\eta - \frac{1}{\mathcal{Z}}\right)u^{3*}, \tag{4.19}$$

$$\begin{aligned}\nabla\cdot\mathbf{p} = &\left[\frac{\partial}{\partial x}\left(\psi p^{11*}\right) + \frac{\partial p^{12*}}{\partial y} + \frac{\partial p^{13*}}{\partial z} - \psi^2\Lambda\mathcal{Z}p^{11*} + 2\psi\kappa\zeta p^{12*} - 2\psi\kappa\eta p^{13*} + \frac{1}{\mathcal{Z}}p^{13*}\right]\mathbf{g}_1^* \\ &+\left[\frac{\partial}{\partial x}\left(\psi p^{12*}\right) + \frac{\partial p^{22*}}{\partial y} + \frac{\partial p^{23*}}{\partial z} - \psi\kappa\zeta p^{11*} - \psi^2\Lambda\mathcal{Z}p^{12*} + \psi\kappa\zeta p^{22*} - \left(\psi\kappa\eta - \frac{2}{\mathcal{Z}}\right)p^{23*}\right]\mathbf{g}_2^* \\ &+\left[\frac{\partial}{\partial x}\left(\psi p^{13*}\right) + \frac{\partial p^{23*}}{\partial y} + \frac{\partial p^{33*}}{\partial z} + \psi\kappa\eta p^{11*} - \frac{1}{\mathcal{Z}}p^{22*} - \psi^2\Lambda\mathcal{Z}p^{13*} + \psi\kappa\zeta p^{23*} - \left(\psi\kappa\eta - \frac{1}{\mathcal{Z}}\right)p^{33*}\right]\mathbf{g}_3^*.\end{aligned} \tag{4.20}$$

4.4 Non-Dimensional Equations

For the ensuing developments it is assumed that the avalanche motion is sufficiently distant from the master curve C. More explicitly, for fixed value $s = const.$, the avalanche domain occupies a region in the plane $S \perp C$ distant from the center of the triad $\{\mathbf{T}, \mathbf{N}, \mathbf{B}\}$, see Fig. 4.6. This then justifies to identify the radial direction with the "thickness" direction and to postulate that the typical "radial thickness" is small relative to a typical (width or) length of the avalanche.

In this Section the coordinate independent equations of Section 3.3.1 are expressed in terms of the simple curvilinear coordinate system introduced in Section 4.3. The physical components of the velocity field $\mathbf{u}$ are defined as u, v and w. Similarly, the physical components of the symmetric pressure tensor $\mathbf{p}$ are $p_{xx}, p_{yy}, p_{zz}, p_{xy}, p_{xz}, p_{yz}$ where the convention that subscripts define contravariant quantities is now dropped , i.e., p_{xx}, etc. are now and henceforth physical components. Also, for notational brevity, from now on, we will simply write $\mathbf{g}_i$ for covariant unit base vectors $\mathbf{g}_i^*$, so that $\mathbf{u} = u\mathbf{g}_x + v\mathbf{g}_y + w\mathbf{g}_z$ defines the physical components u, v, w. The physical variables are non-dimensionalised by using the scalings

$$\begin{aligned}
\left(x, y, z, F^s, F^b, t\right) &= \left(L\hat{x}, L\hat{y}, H\hat{z}, H\hat{F}^s, H\hat{F}^b, (L/g)^{1/2}\,\hat{t}\right), \\
(u, v, w) &= (gL)^{1/2}\,(\hat{u}, \hat{v}, \varepsilon\hat{w}), \\
(p_{xx}, p_{yy}, p_{zz}) &= \varrho_0 gH\,(\hat{p}_{xx}, \hat{p}_{yy}, \hat{p}_{zz}), \\
(p_{xy}, p_{xz}, p_{yz}) &= \varrho_0 gH\mu\,(\hat{p}_{xy}, \hat{p}_{xz}, \hat{p}_{yz}), \\
(g_x, g_y, g_z) &= g\,(\hat{g}_x, \hat{g}_y, \hat{g}_z), \\
(\kappa, \tau) &= (\hat{\kappa}/\mathcal{R}, \hat{\tau}/\mathcal{R}_\tau),
\end{aligned} \tag{4.21}$$

where the hats represent non–dimensional variables. The scalings (4.21) assume that the avalanche has a typical length, L, tangential to the reference surface and a typical thickness, H, normal to it. Furthermore, $\mathcal{R}$ and $\mathcal{R}_\tau$ are, respectively, the typical radius of curvature and torsion of the reference geometry. Assuming a granular static balance, the typical normal pressures at the base of the avalanche are of the order[§] $\varrho_0 gH$, and the Coulomb dry–friction law, (3.3), suggests that the basal shear stresses are of the order $\varrho_0 gH \tan\delta_0$, where δ_0 is a typical basal angle of friction. Also, notice that g_x, g_y and g_z in these equations are dimensional physical components of the gravitational acceleration along the x-, y- and z-coordinates, respectively. Finally, the curvature κ, and torsion τ are assumed to be of order $1/\mathcal{R}$ and $1/\mathcal{R}_\tau$, respectively. These scalings introduce the following *non–dimensional parameters*,

$$\varepsilon = H/L, \quad \lambda = L/\mathcal{R}, \quad \lambda_\tau = L/\mathcal{R}_\tau, \quad \mu = \tan\delta_0, \tag{4.22}$$

where ε is the *aspect ratio* of the avalanche, λ and λ_τ are the *measures of the curvature and torsion* of the reference geometry with respect to the length of the avalanche and μ is the *coefficient of friction* of the granular material associated with the base morphology.

[§]This scaling for the normal pressure tacitly assumes a "hydrostatic nature" of the pressure in a granular heap. This is in fact untypical for granular systems for which the pressure is not the overburden weight but "saturates" after a certain depth. In hoppers etc. the overburden pressure mg over the whole base (A, say) must equal $\int p\,dA = mg = \int \varrho_0 gH\,dA$. So this scaling will always be true, the only exception being if the avalanche is spreading out very rapidly.

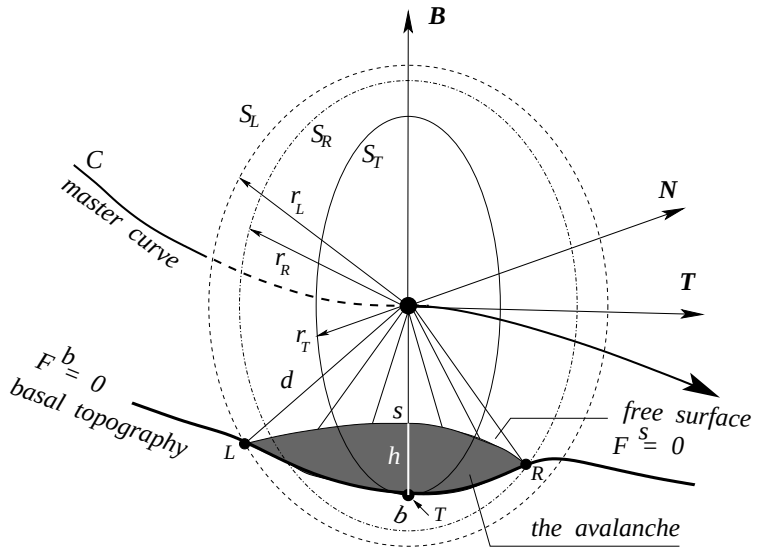

Figure 4.6: For a given value of $s = x$, the avalanche domain in the lateral direction occupies a region in the plane of the circle $S_T \perp C$ distant from the center of the moving triad $\{\mathbf{T}, \mathbf{N}, \mathbf{B}\}$. The concentric and coplanar circles S_T, S_R, and S_L, (with the center at the master curve and radius r_T, r_R, and r_L), respectively, pass through the talweg (T) and the left (L) and right (R) marginal points of the avalanche with its basal topography in the lateral direction. The basal topography $F^b = 0$ and the free surface $F^s = 0$ of the avalanche in this plane section are shown. The depth of the avalanche in this section is represented by a height function $h(x, y, t)$ and is measured in the radial direction. Also shown, for instance, is the distance d of the avalanche from the center line to the circle S_L

4.4.1 Components of the Gravitational Acceleration

The non-dimensional physical components of the gravitational acceleration along the x-, y- and z-coordinates, respectively, can be determined as known functions of curvature and torsion referred to the moving triad of the given master curve. Their derivation is as follows.

Consider the unit orthonormal basis vectors along the coordinate lines:

$$\begin{aligned} \mathbf{g}_x &= \mathbf{T}(x), \\ \mathbf{g}_y &= -\zeta\mathbf{N}(x) + \eta\mathbf{B}(x), \\ \mathbf{g}_z &= \eta\mathbf{N}(x) + \zeta\mathbf{B}(x). \end{aligned} \tag{4.23}$$

The gravitational vector $\mathbf{g}$ can then be written in the form

$$\mathbf{g} = (0, 0, -g) = 0\mathbf{i} + 0\mathbf{j} - g\mathbf{k}, \tag{4.24}$$

where $\{\mathbf{i}, \mathbf{j}, \mathbf{k}\}$ forms the standard Cartesian basis. We need to express $\mathbf{g}$ in terms of $\{\mathbf{g}_i\}$ as follows

$$\begin{aligned} \mathbf{g} &= g_x\mathbf{g}_x + g_y\mathbf{g}_y + g_z\mathbf{g}_z \\ &= g_x\mathbf{T} + g_y\left(-\zeta\mathbf{N} + \eta\mathbf{B}\right) + g_z\left(\eta\mathbf{N} + \zeta\mathbf{B}\right) \\ &= g_x\mathbf{T} - \left(\zeta g_y - \eta g_z\right)\mathbf{N} + \left(\eta g_y + \zeta g_z\right)\mathbf{B} \\ &= g\left[\hat{g}_x\mathbf{T} - \left(\zeta\hat{g}_y - \eta\hat{g}_z\right)\mathbf{N} + \left(\eta\hat{g}_y + \zeta\hat{g}_z\right)\mathbf{B}\right] \end{aligned} \tag{4.25}$$

where $\{g_x, g_y, g_z\} = g\{\hat{g}_x, \hat{g}_y, \hat{g}_z\}$ are the physical components of $\mathbf{g}$ with respect to the basis $\{\mathbf{g}_i\}$. Let (t_i), (b_i) and (n_i); $1 \leq i \leq 3$; be the components of the tangent, normal and binormal unit vectors, respectively, of a given space curve with respect to the standard Cartesian basis $\{\mathbf{i}, \mathbf{j}, \mathbf{k}\}$. We must express the right-hand side of (4.25) in terms of this basis as follows:

$$\begin{aligned}
\mathbf{g} &= g\Big[\hat{g}_x\left(t_1\mathbf{i} + t_2\mathbf{j} + t_3\mathbf{k}\right) - \left(\zeta\hat{g}_y - \eta\hat{g}_z\right)\left(n_1\mathbf{i} + n_2\mathbf{j} + n_3\mathbf{k}\right) + \left(\eta\hat{g}_y + \zeta\hat{g}_z\right)\left(b_1\mathbf{i} + b_2\mathbf{j} + b_3\mathbf{k}\right)\Big] \\
&= g\Big[t_1\hat{g}_x - n_1\left(\zeta\hat{g}_y - \eta\hat{g}_z\right) + b_1\left(\eta\hat{g}_y + \zeta\hat{g}_z\right)\Big]\mathbf{i} \\
&\quad + g\Big[t_2\hat{g}_x - n_2\left(\zeta\hat{g}_y - \eta\hat{g}_z\right) + b_2\left(\eta\hat{g}_y + \zeta\hat{g}_z\right)\Big]\mathbf{j} \\
&\quad + g\Big[t_3\hat{g}_x - n_3\left(\zeta g_y - \eta g_z\right) + b_3\left(\eta\hat{g}_y + \zeta\hat{g}_z\right)\Big]\mathbf{k}. \qquad (4.26)
\end{aligned}$$

Comparing the like terms of this equation with (4.24) we obtain the following set of linear equations in $(\hat{g}_x, \hat{g}_y, \hat{g}_z)$:

$$\begin{aligned}
t_1\hat{g}_x + \left(b_1\eta - n_1\zeta\right)\hat{g}_y + \left(n_1\eta + b_1\zeta\right)\hat{g}_z &= 0, \\
t_2\hat{g}_x + \left(b_2\eta - n_2\zeta\right)\hat{g}_y + \left(n_2\eta + b_2\zeta\right)\hat{g}_z &= 0, \qquad (4.27) \\
t_3\hat{g}_x + \left(b_3\eta - n_3\zeta\right)\hat{g}_y + \left(n_3\eta + b_3\zeta\right)\hat{g}_z &= -1.
\end{aligned}$$

This system can be solved to obtain values for $(\hat{g}_x, \hat{g}_y, \hat{g}_z)$ in terms of t_i, b_i and n_i:

$$\begin{aligned}
\hat{g}_x &= \left[b_1n_2 - b_2n_1\right]/\Delta, \\
\hat{g}_y &= \left[t_2\left(n_1\eta + b_1\zeta\right) - t_1\left(n_2\eta + b_2\zeta\right)\right]/\Delta, \qquad (4.28) \\
\hat{g}_z &= \left[t_1\left(b_2\eta - n_2\zeta\right) - t_2\left(b_1\eta - n_1\zeta\right)\right]/\Delta, \\
\Delta &= t_1\left(n_2b_3 - b_2n_3\right) + t_2\left(b_1n_3 - n_1b_3\right) + t_3\left(n_1b_2 - b_1n_2\right).
\end{aligned}$$

For notational brevity we will replace $(\hat{g}_x, \hat{g}_y, \hat{g}_z)$ simply by (g_x, g_y, g_z), so that g_x, g_y and g_z represent non-dimensional physical components of the gravitational acceleration along down-slope, cross-slope and normal directions, respectively.

4.4.2 Balance Equations

Applying the scalings (4.21) and (4.22), it follows that the non-dimensional curvilinear form of the mass balance equation (4.19) is

$$\frac{\partial}{\partial x}\left(\psi u\right) + \frac{\partial v}{\partial y} + \frac{\partial w}{\partial z} - \varepsilon\lambda\psi^2\Lambda\mathcal{Z}u + \lambda\psi\kappa\zeta v - \left(\varepsilon\lambda\psi\kappa\eta - \frac{1}{\mathcal{Z}}\right)w = 0, \qquad (4.29)$$

where the hats are now and henceforth dropped and

$$\psi = 1/\left(1 - \varepsilon\lambda\kappa\eta\mathcal{Z}\right), \quad \theta = y/\left(\varepsilon z_T\right), \quad \Lambda = \left(\kappa'\eta + \lambda_\tau\kappa\tau\zeta\right). \qquad (4.30)$$

The momentum balance equation (3.2) can be written in curvilinear coordinates by using relation (4.20) to transform the tensor $\mathbf{u} \otimes \mathbf{u}$ and the pressure $\mathbf{p}$. Let g_x, g_y and g_z be the non–dimensional physical components of the gravitational acceleration along the x-, y- and z-coordinates, respectively, as explained and computed in Section 4.4.1. It follows that the non–dimensional momentum components in the downslope, cross–slope and normal directions to the reference surface are, respectively,

$$\begin{aligned}&\frac{\partial u}{\partial t}+\frac{\partial}{\partial x}\left(\psi u^2\right)+\frac{\partial}{\partial y}\left(uv\right)+\frac{\partial}{\partial z}\left(uw\right)-\varepsilon\lambda\psi^2\Lambda\mathcal{Z}u^2+2\lambda\psi\kappa\zeta uv-2\varepsilon\lambda\psi\kappa\eta uw+\frac{1}{\mathcal{Z}}uw \qquad (4.31)\\ &=-\left\{\varepsilon\frac{\partial}{\partial x}(\psi p_{xx})+\varepsilon\mu\frac{\partial}{\partial y}(p_{xy})+\mu\frac{\partial}{\partial z}(p_{xz})-\varepsilon^2\lambda\psi^2\Lambda\mathcal{Z}p_{xx}+2\varepsilon\lambda\mu\psi\kappa\left(\zeta p_{xy}-\eta p_{xz}\right)+\frac{\mu}{\mathcal{Z}}p_{xz}\right\}+g_x,\end{aligned}$$

$$\begin{aligned}&\frac{\partial v}{\partial t}+\frac{\partial}{\partial x}(\psi uv)+\frac{\partial}{\partial y}\left(v^2\right)+\frac{\partial}{\partial z}(vw)-\lambda\psi\kappa\zeta\left(u^2-v^2\right)-\varepsilon\lambda\psi^2\Lambda\mathcal{Z}uv-\left(\varepsilon\lambda\psi\kappa\eta-\frac{2}{\mathcal{Z}}\right)vw \qquad (4.32)\\ &=-\left\{\varepsilon\mu\frac{\partial}{\partial x}(\psi p_{xy})+\varepsilon\frac{\partial}{\partial y}(p_{yy})+\mu\frac{\partial}{\partial z}(p_{yz})-\varepsilon\lambda\psi\kappa\zeta P_y^x-\varepsilon^2\lambda\mu\psi^2\Lambda\mathcal{Z}p_{xy}-\mu\left(\varepsilon\lambda\psi\kappa\eta-\frac{2}{\mathcal{Z}}\right)p_{yz}\right\}+g_y,\end{aligned}$$

$$\begin{aligned}&\varepsilon\left\{\frac{\partial w}{\partial t}+\frac{\partial(\psi uw)}{\partial x}+\frac{\partial(vw)}{\partial y}+\frac{\partial w^2}{\partial z}\right\}+\lambda\psi\kappa\eta u^2-\frac{v^2}{\varepsilon\mathcal{Z}}-\varepsilon\lambda\left(\varepsilon\psi^2\Lambda\mathcal{Z}u-\psi\kappa\zeta v\right)w-\left(\varepsilon^2\lambda\psi\kappa\eta-\frac{\varepsilon}{\mathcal{Z}}\right)w^2 \qquad (4.33)\\ &=-\left\{\varepsilon\mu\frac{\partial}{\partial x}(\psi p_{xz})+\varepsilon\mu\frac{\partial}{\partial y}(p_{yz})+\frac{\partial}{\partial z}(p_{zz})+\varepsilon\lambda\psi\kappa\eta P_z^x-\frac{1}{\mathcal{Z}}P_z^y-\varepsilon^2\lambda\mu\psi^2\Lambda\mathcal{Z}p_{xz}+\varepsilon\lambda\mu\psi\kappa\zeta p_{yz}\right\}+g_z,\end{aligned}$$

where

$$P_y^x=\left(p_{xx}-p_{yy}\right),\ P_z^x=\left(p_{xx}-p_{zz}\right),\ P_z^y=\left(p_{yy}-p_{zz}\right). \qquad (4.34)$$

Further simplification of these equations is possible, but they are left in the given form as this proves to be particularly useful when the free surface and basal boundary conditions are included once the depth-integration process in Section 4.5 is performed.

4.4.3 Kinematic Conditions

The free surface of the avalanche, $F^s(\mathbf{x},t)=0$, and the basal topography over which the avalanche is assumed to slide, $F^b(\mathbf{x},t)=0$, are defined by their respective heights above the curvilinear reference, see Fig. 4.6,

$$F^s\equiv z-s(x,y,t)=0,\quad F^b\equiv -z+b(x,y,t)=0. \qquad (4.35)$$

The functions $F^s(\mathbf{x},t)=0$ and $s(x,y,t)$ are time independent for a stagnant non-moving mass; on the other hand $F^b(\mathbf{x},t)=0$ and $b(x,y,t)$ are only time dependent provided that snow is entrained from the bottom or snow is deposited along the avalanche track. The kinematic surface equations in dimensional form are

$$\frac{\partial F^b}{\partial t}+\mathbf{u}^b\cdot\nabla F^b=0,\quad \frac{\partial F^s}{\partial t}+\mathbf{u}^s\cdot\nabla F^s=0. \qquad (4.36)$$

It is emphasised that $\mathbf{u}^b$ here is the material velocity of particles at the base, but then processes of bed erosion or sedimentation are excluded. In case these processes are included, $\mathbf{u}^b$ in (4.36) would have to be replaced by $\mathbf{w}$, say, the non-material velocity with which the base is moving when erosion from, and deposition of material to, the base are

accounted for. This not being accounted for, we deduce from (4.13), (4.21), (4.22), (4.30), (4.35) and (4.36) the following *non-dimensional* curvilinear kinematic conditions for the basal and free surfaces

$$z = b(x, y, t): \quad \frac{\partial b}{\partial t} + \psi^b u^b \frac{\partial b}{\partial x} + v^b \frac{\partial b}{\partial y} - w^b = 0, \tag{4.37}$$

$$z = s(x, y, t): \quad \frac{\partial s}{\partial t} + \psi^s u^s \frac{\partial s}{\partial x} + v^s \frac{\partial s}{\partial y} - w^s = 0. \tag{4.38}$$

4.4.4 Traction Free Condition at the Free Surface

From the definition (4.13) of the gradient of a scalar field, the traction free condition (3.6) reads

$$\frac{p^{ij}}{\sqrt{g_{(jj)}}} \frac{\partial F^s}{\partial x^j} \mathbf{g}_i = 0. \tag{4.39}$$

Hence, the traction free boundary condition at the free surface of the avalanche has downslope, cross-slope and normal physical components as follows

$$\begin{aligned} -\varepsilon\psi^s p^s_{xx} \frac{\partial s}{\partial x} - \varepsilon\mu p^s_{xy} \frac{\partial s}{\partial y} + \mu p^s_{xz} &= 0, \\ -\varepsilon\mu\psi^s p^s_{yx} \frac{\partial s}{\partial x} - \varepsilon p^s_{yy} \frac{\partial s}{\partial y} + \mu p^s_{yz} &= 0, \\ -\varepsilon\mu\psi^s p^s_{zx} \frac{\partial s}{\partial x} - \varepsilon\mu p^s_{zy} \frac{\partial s}{\partial y} + p^s_{zz} &= 0, \end{aligned} \tag{4.40}$$

written here again in *dimensionless* form.

4.4.5 Coulomb Sliding Law at the Base

From (4.14), (4.21), (4.22) and (4.30), we obtain the *non–dimensional form* of the gradient of the basal surface as follows

$$\nabla F^b = \varepsilon\psi^b \frac{\partial b}{\partial x} \mathbf{g}_x + \varepsilon \frac{\partial b}{\partial y} \mathbf{g}_y - \mathbf{g}_z. \tag{4.41}$$

The Coulomb basal sliding law (3.7) states that the basal shear traction is proportional to the pressure perpendicular to the surface, the factor of proportionality being the bed friction coefficient $\tan\delta$. It implies the relation

$$\underbrace{\mathbf{p}^b\mathbf{n}^b - \left(\mathbf{n}^b \cdot \mathbf{p}^b\mathbf{n}^b\right)\mathbf{n}^b}_{\text{negative shear traction}} = \left(\frac{\mathbf{u}^b}{|\mathbf{u}^b|}\right) \underbrace{\left(\mathbf{n}^b \cdot \mathbf{p}^b\mathbf{n}^b\right)}_{\substack{\text{pressure} \\ \text{normal to} \\ \text{surface}}} \underbrace{\tan\delta}_{\substack{\text{friction} \\ \text{angle } \delta}}, \tag{4.42}$$

or

$$\mathbf{p}^b\mathbf{n}^b = \left(\mathbf{n}^b \cdot \mathbf{p}^b\mathbf{n}^b\right) \left\{ \left(\mathbf{u}^b/|\mathbf{u}^b|\right) \tan\delta + \mathbf{n}^b \right\}. \tag{4.43}$$

It follows from this and (4.40) and (4.41) that the *dimensionless* downslope, cross-slope and normal components, respectively, of the sliding law (traction vector) read

$$\begin{aligned}
\varepsilon\psi^b p^b_{xx}\frac{\partial b}{\partial x} + \varepsilon\mu p^b_{xy}\frac{\partial b}{\partial y} - \mu p^b_{xz} &= \left(\mathbf{n}^b\cdot\mathbf{p}^b\mathbf{n}^b\right)\left(\Delta_b\frac{u^b}{|\mathbf{u}^b|}\tan\delta + \varepsilon\psi^b\frac{\partial b}{\partial x}\right),\\
\varepsilon\mu\psi^b p^b_{yx}\frac{\partial b}{\partial x} + \varepsilon p^b_{yy}\frac{\partial b}{\partial y} - \mu p^b_{yz} &= \left(\mathbf{n}^b\cdot\mathbf{p}^b\mathbf{n}^b\right)\left(\Delta_b\frac{v^b}{|\mathbf{u}^b|}\tan\delta + \varepsilon\frac{\partial b}{\partial y}\right),\\
\varepsilon\mu\psi^b p^b_{zx}\frac{\partial b}{\partial x} + \varepsilon\mu p^b_{zy}\frac{\partial b}{\partial y} - p^b_{zz} &= \left(\mathbf{n}^b\cdot\mathbf{p}^b\mathbf{n}^b\right)\left(\Delta_b\frac{\varepsilon w^b}{|\mathbf{u}^b|}\tan\delta - 1\right),
\end{aligned} \tag{4.44}$$

where $|\mathbf{u}| = (u^2+v^2+\varepsilon^2w^2)^{1/2}$, the basal unit normal vector $\mathbf{n}^b$ is given by $\Delta_b\mathbf{n}^b = \nabla F^b$, $\Delta_b := |\nabla F^b|$, and the associated normalisation factor is

$$\Delta_b = \left\{1 + \varepsilon^2\left(\psi^b\right)^2\left(\frac{\partial b}{\partial x}\right)^2 + \varepsilon^2\left(\frac{\partial b}{\partial y}\right)^2\right\}^{1/2}. \tag{4.45}$$

Note: *Notice that this dry friction law could be extended to incorporate a velocity dependent contribution, but given the many experimental facts that a large number of laboratory experiments and the observations of the field events did not press for an alteration of the sliding law, this will not be done here. For related topics, also see [93, 94].*

This completes the transformation from the coordinate independent form of Section 3.3.1 to curvilinear coordinates of Section 4.3 using the non-dimensional variables defined in (4.21) and (4.22).

4.5 Depth Integration

The distance between the free surface, $s(x,y,t)$ and the basal topography, $b(x,y,t)$, defines the thickness, or depth, of the avalanche

$$h(x,y,t) = s(x,y,t) - b(x,y,t), \tag{4.46}$$

measured in the normal (radial) direction within the plane normal to the reference curve, see Fig. 4.6. A *crucial step* in deriving the equations of motion for the evolution of the shallow geometry of the granular material is the process of integration of the mass and the momentum balance equations through this thickness. In order to perform this step, it is useful to define the mean value of a function $f = f(x,y,z,t)$ over the avalanche thickness

$$\bar{f}(x,y,t) = \frac{1}{h(x,y,t)}\int_{b(x,y,t)}^{s(x,y,t)} f(x,y,z,t)dz, \tag{4.47}$$

where the over-bar is a shorthand notation for the mean of the depth-integrated value divided by the depth.

In the process of depth-integration, we need Leibniz' rule to change the order of integration and differentiation. According to this rule, if $G(x,t)$ and $\partial G(x,t)/\partial t$ are continuous

functions with respect to x and t and if the functions $a(t)$ and $b(t)$ are differentiable with respect to t, then the following holds true

$$\frac{d}{dt}\int_{a(t)}^{b(t)} G(x,t)dx = \int_{a(t)}^{b(t)} \frac{\partial}{\partial t}\left(G(x,t)\right)dx + \left[G(x,t)\frac{dx}{dt}\right]_{a(t)}^{b(t)}, \tag{4.48}$$

where the square bracket defines the difference of the enclosed function at the two limiting points of integration, $[f]_a^b = f^b - f^a$.

On using Leibniz' rule (4.48) the mass balance (4.29) is integrated through the avalanche depth. This yields

$$\begin{aligned}&\int_b^s \left\{\frac{\partial}{\partial x}(\psi u) + \frac{\partial v}{\partial y} + \frac{\partial w}{\partial z} - \varepsilon\lambda\psi^2\Lambda\mathcal{Z}u + \lambda\psi\kappa\zeta v - \left(\varepsilon\lambda\psi\kappa\eta - \frac{1}{\mathcal{Z}}\right)w\right\}dz \qquad (4.49)\\ &= \frac{\partial}{\partial x}\left(h\overline{\psi u}\right) + \frac{\partial}{\partial y}\left(h\overline{v}\right) - \left[\psi u\frac{\partial z}{\partial x} + v\frac{\partial z}{\partial y} - w\right]_b^s - \varepsilon\lambda h\overline{\psi^2\Lambda\mathcal{Z}u} + \lambda h\overline{\psi\kappa\zeta v} - h\overline{\left(\varepsilon\lambda\psi\kappa\eta - \frac{1}{\mathcal{Z}}\right)w}.\end{aligned}$$

The function contained in square brackets in (4.49) has a number of terms in common with the equations expressing the kinematic boundary conditions (4.37) and (4.38). From (4.37), (4.38) and (4.46) we obtain

$$0 = \frac{\partial h}{\partial t} + \left[\psi u\frac{\partial z}{\partial x} + v\frac{\partial z}{\partial y} - w\right]_b^s. \tag{4.50}$$

From (4.49) and (4.50) it therefore follows that the depth-integrated form of the mass balance (4.29) takes the form

$$\frac{\partial h}{\partial t} + \frac{\partial}{\partial x}\left(h\overline{\psi u}\right) + \frac{\partial}{\partial y}\left(h\overline{v}\right) - \varepsilon\lambda h\overline{\psi^2\Lambda\mathcal{Z}u} + \lambda h\overline{\psi\kappa\zeta v} - h\overline{\left(\varepsilon\lambda\psi\kappa\eta - \frac{1}{\mathcal{Z}}\right)w} = 0, \tag{4.51}$$

valid for a density preserving material. Notice, it does *not* possess "usual" conservation law structure.

The process of depth-integration of the momentum balance equations (4.31)–(4.33) is performed in a number of steps. Integrating the first four terms of the left-hand side of (4.31) (the downslope acceleration) and then using kinematic conditions (4.37) and (4.38), we have

$$\begin{aligned}&\int_b^s \left\{\frac{\partial u}{\partial t} + \frac{\partial}{\partial x}\left(\psi u^2\right) + \frac{\partial}{\partial y}\left(uv\right) + \frac{\partial}{\partial z}\left(uw\right)\right\}dz\\ &= \frac{\partial}{\partial t}\left(h\overline{u}\right) + \frac{\partial}{\partial x}\left(h\overline{\psi u^2}\right) + \frac{\partial}{\partial y}\left(h\overline{uv}\right) - \left[u\left(\frac{\partial z}{\partial t} + \psi u\frac{\partial z}{\partial x} + v\frac{\partial z}{\partial y} - w\right)\right]_b^s\\ &= \frac{\partial}{\partial t}\left(h\overline{u}\right) + \frac{\partial}{\partial x}\left(h\overline{\psi u^2}\right) + \frac{\partial}{\partial y}\left(h\overline{uv}\right). \qquad (4.52)\end{aligned}$$

Similarly, the first three terms of the right–hand side of (4.31), after integrating and employing $(4.40)_1$ and $(4.44)_1$, reduces to

$$\begin{aligned}
&\int_b^s \left\{ \varepsilon \frac{\partial}{\partial x}\left(\psi p_{xx}\right) + \varepsilon\mu \frac{\partial}{\partial y}\left(p_{xy}\right) + \mu \frac{\partial}{\partial z}\left(p_{xz}\right) \right\} dz \\
&= \left[\varepsilon \frac{\partial}{\partial x}\left(h\overline{\psi p_{xx}}\right) + \varepsilon\mu \frac{\partial}{\partial y}\left(h\overline{p_{xy}}\right) \right] - \left[\varepsilon\psi p_{xx}\frac{\partial z}{\partial x} + \varepsilon\mu p_{xy}\frac{\partial z}{\partial y} - \mu p_{xz} \right]_b^s \\
&= \varepsilon \frac{\partial}{\partial x}\big(h\overline{\psi p_{xx}}\,\big) + \varepsilon\mu \frac{\partial}{\partial y}\big(h\overline{p_{xy}}\big) + \big(\mathbf{n}^b\cdot\mathbf{p}^b\mathbf{n}^b\big)\left(\Delta_b \frac{u^b}{|\mathbf{u}^b|}\tan\delta + \varepsilon\psi^b\frac{\partial b}{\partial x}\right), \qquad (4.53)
\end{aligned}$$

where the COULOMB dry–friction law and the down–slope component of the basal normal pressure enter through the boundary conditions. In a similar fashion we can derive corresponding expressions for the depth–integrated cross–slope and normal components of the momentum balances. It then follows that the depth–integrated down–slope, cross–slope and normal components of the momentum balances, respectively, are

$$\begin{aligned}
&\frac{\partial}{\partial t}\left(h\overline{u}\right) + \frac{\partial}{\partial x}\left(h\overline{\psi u^2}\right) + \frac{\partial}{\partial y}\left(h\overline{uv}\right) - \varepsilon\lambda h\overline{\psi^2\Lambda\mathcal{Z}u^2} + 2\lambda\kappa h\overline{\psi\zeta uv} - 2\varepsilon\lambda\kappa h\overline{\psi\eta uw} + h\overline{\left(\frac{uw}{\mathcal{Z}}\right)} \\
&= -\left(\Delta_b\frac{u^b}{|\mathbf{u}^b|}\tan\delta + \varepsilon\psi^b\frac{\partial b}{\partial x}\right)\big(\mathbf{n}^b\cdot\mathbf{p}^b\mathbf{n}^b\big) - \varepsilon\frac{\partial}{\partial x}\big(h\overline{\psi p_{xx}}\big) - \varepsilon\mu\frac{\partial}{\partial y}\big(h\overline{p_{xy}}\big) \\
&\quad + \varepsilon^2\lambda h\overline{\psi^2\Lambda\mathcal{Z}p_{xx}} - 2\varepsilon\lambda\mu\kappa h\overline{\psi\left(\zeta p_{xy} - \eta p_{xz}\right)} - \mu h\overline{\left(\frac{p_{xz}}{\mathcal{Z}}\right)} + hg_x, \qquad (4.54)
\end{aligned}$$

$$\begin{aligned}
&\frac{\partial}{\partial t}\left(h\overline{v}\right) + \frac{\partial}{\partial x}\left(h\overline{\psi uv}\right) + \frac{\partial}{\partial y}\left(h\overline{v^2}\right) - \lambda\kappa h\overline{\psi\zeta\left(u^2 - v^2\right)} - \varepsilon\lambda h\left(\overline{\psi^2\Lambda\mathcal{Z}uv} - \kappa\overline{\psi\eta vw}\right) + 2h\overline{\left(\frac{vw}{\mathcal{Z}}\right)} \\
&= -\left(\Delta_b\frac{v^b}{|\mathbf{u}^b|}\tan\delta + \varepsilon\frac{\partial b}{\partial y}\right)\left(\mathbf{n}^b\cdot\mathbf{p}^b\mathbf{n}^b\right) - \varepsilon\mu\frac{\partial}{\partial x}\left(h\overline{\psi p_{xy}}\right) - \varepsilon\frac{\partial}{\partial y}\left(h\overline{p_{yy}}\right) + \varepsilon\lambda\kappa h\overline{\psi\zeta P_y^x} \\
&\quad + \varepsilon^2\lambda\mu h\overline{\psi^2\Lambda\mathcal{Z}p_{xy}} + \varepsilon\lambda\mu\kappa h\overline{\psi\eta p_{yz}} + 2\mu h\overline{\left(\frac{p_{yz}}{\mathcal{Z}}\right)} + hg_y, \qquad (4.55)
\end{aligned}$$

$$\begin{aligned}
&\varepsilon\left\{\frac{\partial}{\partial t}\left(h\overline{w}\right) + \frac{\partial}{\partial x}\left(h\overline{\psi uw}\right) + \frac{\partial}{\partial y}\left(h\overline{vw}\right)\right\} + \lambda\kappa h\overline{\psi\eta u^2} - \frac{h}{\varepsilon}\overline{\left(\frac{v^2}{\mathcal{Z}}\right)} - \varepsilon^2\lambda h\overline{\psi^2\Lambda\mathcal{Z}uw} \\
&\quad + \varepsilon\lambda\kappa h\overline{\psi\zeta vw} - \varepsilon^2\lambda\kappa h\overline{\psi\eta w^2} + \varepsilon h\overline{\left(\frac{w^2}{\mathcal{Z}}\right)} \\
&= -\left(\Delta_b\frac{\varepsilon w^b}{|\mathbf{u}^b|}\tan\delta - 1\right)\left(\mathbf{n}^b\cdot\mathbf{p}^b\mathbf{n}^b\right) - \varepsilon\mu\frac{\partial}{\partial x}\left(h\overline{\psi p_{xz}}\right) - \varepsilon\mu\frac{\partial}{\partial y}\left(h\overline{p_{yz}}\right) \qquad (4.56) \\
&\quad - \varepsilon\lambda\kappa h\overline{\psi\left(\eta P_z^x + \mu\zeta p_{yz}\right)} + h\overline{\left(\frac{p_{yy}}{\mathcal{Z}}\right)} + \varepsilon^2\lambda\mu h\overline{\psi^2\Lambda\mathcal{Z}p_{xz}} - h\overline{\left(\frac{p_{zz}}{\mathcal{Z}}\right)} + hg_z.
\end{aligned}$$

The formal depth-integration process is now complete. The depth-integrated mass balance (4.51), and the downslope and cross–slope momentum balances (4.54) and (4.55), will form *the basis of the shallow granular motion*. The depth integrated normal component of the momentum equation, (4.56) will thereby serve as an *auxiliary equation defining the pressure*. This will now be made clear.

4.6 Ordering

Equations (4.51), (4.54)-(4.56) constitute four scalar field equations for h, u, v and w as unknowns. However, they contain more than just these unknowns because many "correction terms" arise which are thickness averages of product quantities of h, u, v and w as well as stress components. The number of these unknown variables can be reduced by introducing a further *approximation* that is based on the ordering of the various terms arising in the stated equations. Such orders of magnitudes are now assumed for the parameters λ, λ_τ and μ. Realistic avalanche lengths are generally larger than typical curvatures and torsions of the topography. Of course, this is not unanimously so, but $0 < \lambda, \lambda_\tau < 1$ is almost everywhere correct. Similarly δ_0 as a typical friction angle is smaller than 45° (usually between 20° and 30°, both in field and in laboratory). So also $0 < \mu < 1$ must hold. Since the aspect ratio is generally much smaller than unity, from (4.22) it follows that such corrections are fulfilled for

$$\varepsilon \ll 1, \quad \lambda = O\left(\varepsilon^{\alpha}\right), \quad \lambda_\tau = O\left(\varepsilon^{\alpha_\tau}\right), \quad \mu = O\left(\varepsilon^{\beta}\right), \tag{4.57}$$

where $0 < \alpha, \alpha_\tau, \beta < 1$ are realistic for typical reference surface curvature, torsion and coefficients of basal friction. As long as no formal perturbation expansion involving higher order terms is pursued the exponents α, α_τ and β need not further be specified except $\alpha \neq 1,\ \alpha_\tau \neq 1,\ \beta \neq 1$. As typical values of these parameters we can take $\alpha = 1/2,\ \alpha_\tau = 1/2,\quad \beta = 1/2$, $\varepsilon = 1/100$ and $\mu = 1/10$. Therefore, the functions ψ and Δ_b in (4.30) and (4.45), respectively, can be estimated by

$$\psi = 1 + O\left(\varepsilon^{1+\alpha}\right), \quad \Delta_b = 1 + O\left(\varepsilon^{2}\right). \tag{4.58}$$

With these orderings, the depth-integrated mass balance equation (4.51) reduces to

$$\frac{\partial h}{\partial t} + \frac{\partial}{\partial x}\left(h\overline{u}\right) + \frac{\partial}{\partial y}\left(h\overline{v}\right) + \lambda h\overline{\kappa\zeta v} - h\overline{\left(\frac{w}{\mathcal{Z}}\right)} = 0, \tag{4.59}$$

to order $(\varepsilon^{1+\alpha})$.

The downslope and cross-slope components of the depth-integrated momentum balances (4.54) and (4.55) must be approximated to leading (ε^0) and first (ε^1) order in the small parameter ε in order to obtain *a realizable theory which includes some constitutive properties of granular material*. These equations contain a common term that is multiplied by the factor $\mathbf{n}^b \cdot \mathbf{p}^b\mathbf{n}^b$. From the normal component of the momentum balance (4.56), it follows that to *leading order*

$$\begin{aligned} \mathbf{n}^b \cdot \mathbf{p}^b\mathbf{n}^b &= \lambda\kappa h\overline{\psi\eta u^2} + hC - hg_z + O\left(\varepsilon\right) \\ &= hC - hg_z + O\left(\varepsilon^{\gamma}\right), \end{aligned} \tag{4.60}$$

where

$$C = \overline{\left(\frac{p_{zz}}{\mathcal{Z}}\right)} - \overline{\left(\frac{p_{yy}}{\mathcal{Z}}\right)} - \overline{\left(\frac{v^2}{\varepsilon\mathcal{Z}}\right)}, \tag{4.61}$$

and $\gamma = \min(\alpha, \alpha_\tau, \beta)$. The normal component of the *local momentum balance* (4.33) also reduces to

$$\frac{\partial}{\partial z}\left(p_{zz}\right) = \frac{p_{yy}}{\mathcal{Z}} - \frac{p_{zz}}{\mathcal{Z}} + \frac{v^2}{\varepsilon\mathcal{Z}} + g_z + O\left(\varepsilon^{\gamma}\right). \tag{4.62}$$

Integrating this from $z' = z$ to $z' = s$ we obtain (with $\mathcal{Z}' = z' + z_T$)

$$p_{zz} = -\int_z^s \left\{ \frac{p_{yy}}{\mathcal{Z}'} - \frac{p_{zz}}{\mathcal{Z}'} + \frac{v^2}{\varepsilon \mathcal{Z}'} + g_z \right\} dz' + O\left(\varepsilon^\gamma\right), \tag{4.63}$$

from which it follows that

$$p^b_{zz} = hC - hg_z + O\left(\varepsilon^\gamma\right). \tag{4.64}$$

This, together with $(4.44)_3$ and (4.60), eventually proves the *consistency* of our computations, namely that

$$\left(\mathbf{n}^b \cdot \mathbf{p}^b \mathbf{n}^b\right) = p^b_{zz}. \tag{4.65}$$

In the SH-theory a linear variability of the pressure with depth is assumed. This is fulfilled if

$$\int_z^s \left\{ \frac{p_{yy}}{\mathcal{Z}'} - \frac{p_{zz}}{\mathcal{Z}'} + \frac{v^2}{\varepsilon \mathcal{Z}'} \right\} dz' = O\left(\varepsilon^\gamma\right), \tag{4.66}$$

so that it follows from (4.63) that

$$p_{zz} = -\left(s - z\right) g_z + O\left(\varepsilon^\gamma\right), \quad p^b_{zz} = -hg_z + O\left(\varepsilon^\gamma\right). \tag{4.67}$$

Since we are deriving depth–averaged model equations we must somehow eliminate the effects of the normal component w of the velocity field and the normal coordinate z from the balance equations. In typical avalanche flows the dominant deformation takes place mainly in the down–hill direction. It is therefore legitimate to assume that p_{xz} and p_{yz} are of order ε and that their variations with z are negligible. With these assumptions, we have the following results:

$$\overline{\left(p_{xz}/\mathcal{Z}\right)} = O\left(\varepsilon\right), \quad \overline{\left(p_{yz}/\mathcal{Z}\right)} = O\left(\varepsilon\right). \tag{4.68}$$

Due to the depth-averaging and the Boussinesq assumption (see later, Section 4.8), we may also assume that $\overline{(uw/\mathcal{Z})}, \overline{(vw/\mathcal{Z})}, \overline{(w/\mathcal{Z})}$ are negligible. Moreover, since we consider shallow–geometry of the basal topography, for shallow curvature and torsion , we may also consider $\lambda\kappa\zeta$ to be negligible.

Summarising the above analysis and restricting considerations to $O\left(\varepsilon^1\right)$-terms we deduce from (4.57), (4.58), (4.60), (4.65), (4.67) and (4.68), that the mass balance (4.59) and the downslope and cross-slope momentum components (4.54) and (4.55) reduce to

$$\frac{\partial h}{\partial t} + \frac{\partial}{\partial x}\left(h\overline{u}\right) + \frac{\partial}{\partial y}\left(h\overline{v}\right) = 0, \tag{4.69}$$

$$\begin{aligned} &\frac{\partial}{\partial t}\left(h\overline{u}\right) + \frac{\partial}{\partial x}\left(h\overline{u^2}\right) + \frac{\partial}{\partial y}\left(h\overline{uv}\right) \\ &\quad = hg_x - h\frac{u^b}{|\mathbf{u}^b|}\tan\delta\left[-g_z + \lambda\kappa\eta\overline{u^2}\right] + \varepsilon h g_z \frac{\partial b}{\partial x} - \varepsilon\frac{\partial}{\partial x}\left(h\overline{p_{xx}}\right), \end{aligned} \tag{4.70}$$

$$\begin{aligned} &\frac{\partial}{\partial t}\left(h\overline{v}\right) + \frac{\partial}{\partial x}\left(h\overline{uv}\right) + \frac{\partial}{\partial y}\left(h\overline{v^2}\right) \\ &\quad = hg_y - h\frac{v^b}{|\mathbf{u}^b|}\tan\delta\left[-g_z + \lambda\kappa\eta\overline{u^2}\right] + \varepsilon h g_z \frac{\partial b}{\partial y} - \varepsilon\frac{\partial}{\partial y}\left(h\overline{p_{yy}}\right), \end{aligned} \tag{4.71}$$

correct to order $\varepsilon^{1+\gamma}$.

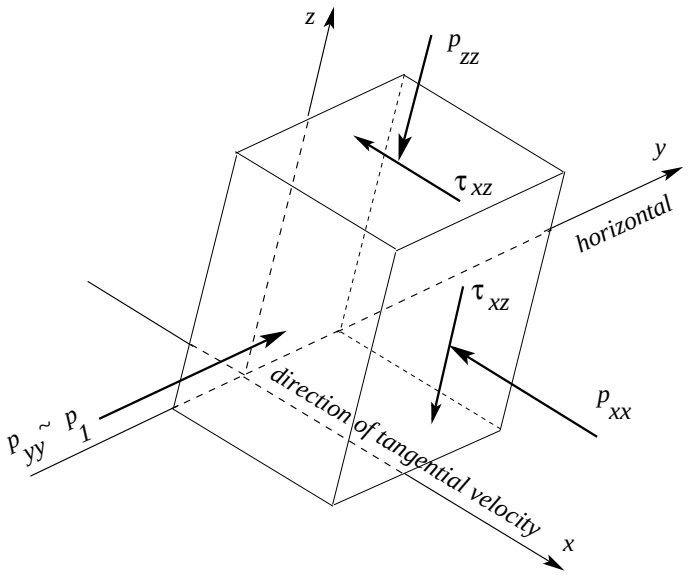

Figure 4.7: Infinitesimal cubic element cut out of the avalanche with surfaces perpendicular to the coordinates. The motion predominantly is in the direction of steepest descent and the dominant shearing is parallel to the xz-plane. This gives rise to the dominant shear stresses p_{xz} and normal pressures p_{xx}, p_{yy}, p_{zz}. Shear stresses p_{yz} and p_{xy} also arise but much smaller than p_{xz}. Thus p_{yy} equals approximately to p_1, one of the principal stresses. (When p_{yz} and p_{xy} vanish exactly then p_{yy} is exactly p_1). The other two principal stresses, p_2 and p_3, act on surface elements of which the surface normals lie in the (xz)-plane

4.7 Closure Property

Further reduction of equations (4.70) and (4.71) requires "constitutive information" about the pressure tensor $\mathbf{p}$ and the depth integrated tangential velocity $\mathbf{u}$. Note that the pressure p_{zz} need only be approximated to order ε^γ as it is used to simplify the depth integrated downslope and cross-slope pressure terms $\overline{p_{xx}}$ and $\overline{p_{yy}}$, which are already order ε terms in equations (4.70) and (4.71).

The SH-theory assumes that a very simple state of stress prevails within the avalanche. Following common practice in soil mechanics we assume that the horizontal pressure terms p_{xx} and p_{yy} can be expressed in terms of the overburden pressure p_{zz} with the aid of the MOHR-circle. This holds at the base and at the stress free surface. So its validity through depth is justified by the continuity requirement. Because the predominant shearing takes place in vertical surfaces parallel to the direction of tangential velocity, it may as a rough approximation be justified to assume that the lateral confinement pressure p_{yy} is close to a principal stress, p_1 say, see Fig. 4.7. Furthermore, it shall be assumed that one of the other principal stresses acting in the (x, z)-surface, p_2 and p_3, equals p_1. This is an ad-hoc assumption that is not guaranteed by any physical argument[¶], but it reduces the three MOHR-circles that describe all possible combinations of normal stresses and shear stresses to only one MOHR-circle as in the case in two dimensions. Thus, to a given stress state $\left(p^b_{xx}, p^b_{xz}\right)$ at the base, two MOHR stress circles can be constructed to satisfy both

[¶]This assumption is equivalent to the statement that, of the three MOHR circles in a three-dimensional stress state, one circle collapses to a point.

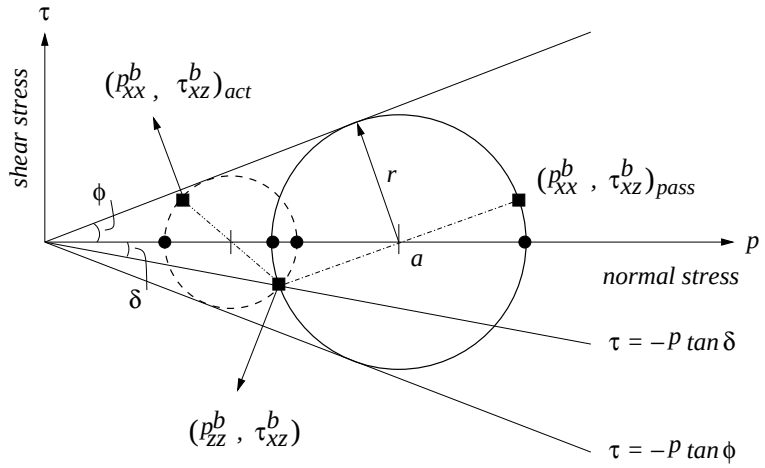

Figure 4.8: MOHR-circle-diagram representing the stress state within the avalanche. The yield criterion corresponds to the two straight lines at angles $\pm\phi$ to the horizontal. Similarly, the COULOMB basal dry friction is indicated by the line at an angle $-\delta$ to the horizontal. The *passive* basal stress state is indicated by the solid circle of radius r and the center at $p = a$. The circle is both tangent to the yield curves and passes through the point $(p_{zz}, -p_{zz}\tan\delta)$. The brocken-line-circle represents a second *active* stress state that also satisfies these conditions. ■ indicate the possible stress states in the xz-plane, ● show possible stress states for p_{yy}

the basal sliding law and the internal yield criterion simultaneously. Their construction is shown in Fig. 4.8.

The principal stresses, p_2 and p_3 in the xz-plane are given by

$$(p_2,\ \ p_3) = \frac{1}{2}\,(p_{xx} + p_{zz}) \pm \frac{1}{2}\sqrt{(p_{xx} - p_{zz})^2 + 4\mu^2 p_{xz}^2}, \tag{4.72}$$

and the cross-slope principal stress $p_{yy} = p_2$ or p_3 depending on the nature of deformation. In the original works of SAVAGE & HUTTER [112, 113], the basal normal pressure equals p^b_{zz} and the shear stress equals $-p^b_{xz}$. The basal downslope pressure p^b_{xx} can therefore assume two values, one on the smaller circle, $p^b_{xx} \le p^b_{zz}$, and one on the larger circle $p^b_{xx} > p^b_{zz}$, that are related to *active* and *passive* stress states, respectively. Since there are four possible values for the principal stresses, p^b_x and p^b_z, there are four values for the basal cross-slope pressure p^b_{yy}. The earth pressure coefficients K^b_x and K^b_y are defined as follows:

$$K^b_x = \frac{p^b_{xx}}{p^b_{zz}}, \quad K^b_y = \frac{p^b_{yy}}{p^b_{zz}}. \tag{4.73}$$

To determine the values of these pressure coefficients, SAVAGE & HUTTER [112, 113] and HUTTER et al. [49] used elementary geometrical arguments and the MOHR-circle representation (4.72), see also Fig. 4.8, as a function of the internal and basal angles of friction, to derive

$$K^b_{x_{act/pas}} = 2\sec^2\phi\left\{1 \mp \left(1 - \cos^2\phi\sec^2\delta\right)^{1/2}\right\} - 1, \tag{4.74}$$

$$\left(K^x_{y_{act/pas}}\right)^b = \frac{1}{2}\left\{\left(K^b_x + 1\right) \mp \left(\left(K^b_x - 1\right)^2 + 4\tan^2\delta\right)^{1/2}\right\}, \tag{4.75}$$

which are real for $\delta \leq \phi$.

Remark: *Otherwise (i.e., for $\delta > \phi$) basal sliding will not be effective and there would be a strong shearing throughout the depth of the body and the motion will be dominated by internal slip. This, probably, is not the case in granular avalanches.*

To uniquely determine the value of the earth pressure coefficient associated with a particular deformation the earth pressure coefficient K_x is defined to be *active* (upper sign) or *passive* (lower sign) according to whether the downslope motion is *dilatational* or *compressional* as given by the following equation

$$K^b_x = \begin{cases} K_{x_{act}}, & \partial u/\partial x \geq 0, \\ \\ K_{x_{pas}}, & \partial u/\partial x < 0. \end{cases} \tag{4.76}$$

Analogously, the earth pressure coefficients in the lateral direction are computed by considering whether the downslope and cross-slope deformation are dilatational or compressional:

$$K^b_y = \begin{cases} K^{x_{act}}_{y_{act}}, & \partial u/\partial x \geq 0, \quad \partial v/\partial y \geq 0, \\ \\ K^{x_{act}}_{y_{pas}}, & \partial u/\partial x \geq 0, \quad \partial v/\partial y < 0, \\ \\ K^{x_{pas}}_{y_{act}}, & \partial u/\partial x < 0, \quad \partial v/\partial y \geq 0, \\ \\ K^{x_{pas}}_{y_{pas}}, & \partial u/\partial x < 0, \quad \partial v/\partial y < 0. \end{cases} \tag{4.77}$$

At the traction free surface of the avalanche the MOHR-COULOMB yield criterion collapses to order ε^γ to a single point and the downslope and cross-slope normal surface pressures are

$$p^s_{xx} = 0 + O\left(\varepsilon^\gamma\right), \quad p^s_{yy} = 0 + O\left(\varepsilon^\gamma\right). \tag{4.78}$$

Having the values of p_{xx} and p_{zz} at the base and the free surface, intermediate values are now interpolated accordingly. The SH-theory assumes that the downslope and cross-slope pressures vary linearly with normal pressure through the avalanche depth. This is achieved to leading order by the following expression

$$p_{xx} = K^b_x p_{zz} + O\left(\varepsilon^\gamma\right), \quad p_{yy} = K^b_y p_{zz} + O\left(\varepsilon^\gamma\right). \tag{4.79}$$

Substituting for the normal pressure p_{zz} from (4.67) and integrating through the avalanche depth the depth-integrated pressures in the downslope and cross-slope directions are, respectively, given by

$$h\overline{p_{xx}} = K^b_x g_z \int_b^s (z - s)\, dz = K^b_x g_z \left[\frac{z^2}{2} - sz\right]_b^s = -\frac{1}{2}K^b_x h^2 g_z + O\left(\varepsilon^\gamma\right), \tag{4.80}$$

$$h\overline{p_{yy}} = K^b_y g_z \int_b^s (z - s)\, dz = K^b_y g_z \left[\frac{z^2}{2} - sz\right]_b^s = -\frac{1}{2}K^b_y h^2 g_z + O\left(\varepsilon^\gamma\right). \tag{4.81}$$

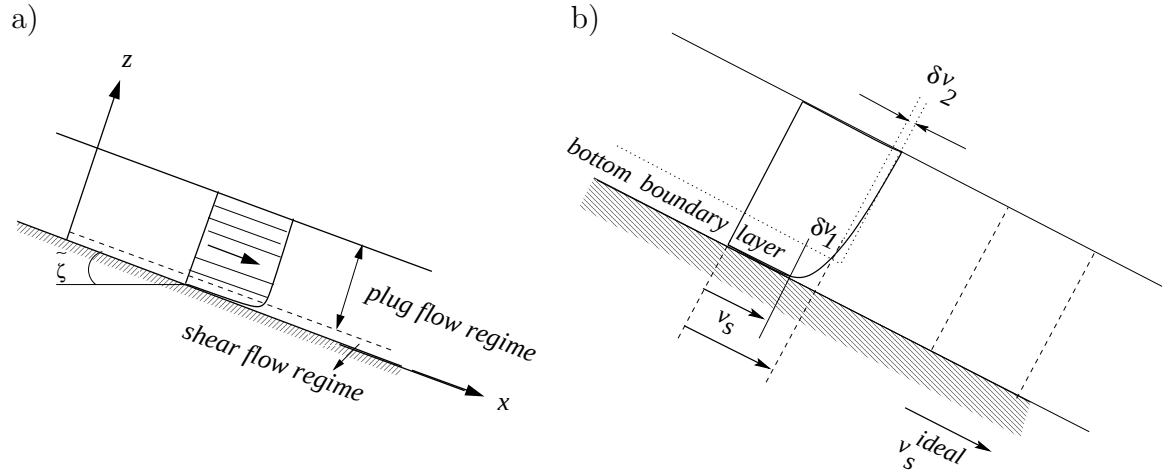

Figure 4.9: a) Gravity-driven granular motion with a large plug flow regime lying atop of a thin shear flow regime on the basal surface. The shear layer is magnified. b) Velocity profile in a gravity driven shear flow. The velocity at a certain depth is composed of a sliding contribution, v_s, a contribution of strong shearing in a bottom boundary layer, δv_1 and a very small shearing contribution δv_2 in the larger top layer. In general, the velocity of flowing material can be idealised by taking an approximate sliding velocity at the base

4.8 Nearly Uniform Flow Profile

In a *depth integrated hydraulic model* such as the SAVAGE-HUTTER-theory there is no possibility to evaluate the depth variation of the velocity. It must rather be postulated, and here it is assumed that the velocity profiles are approximately uniform through the avalanche depth so that *mostly sliding and little differential shearing* takes place. Figure 4.9a,b explain how the velocity of the flowing material can be idealised by considering an approximate sliding velocity at the base. In the literature such an assumption has first been introduced by BOUSSINESQ [7] and is mathematically written in the following form

$$\overline{u} = u^b + O\left(\varepsilon^{1+\gamma}\right), \qquad \overline{v} = v^b + O\left(\varepsilon^{1+\gamma}\right). \tag{4.82}$$

This means that the characteristic mean velocities in the longitudinal and lateral directions can be approximated by their basal counterparts to order $\varepsilon^{1+\gamma}$. The velocity product can then be factorised as

$$\overline{uv} = u^b v^b + O\left(\varepsilon^{1+\gamma}\right) = \overline{u}\,\overline{v} + O\left(\varepsilon^{1+\gamma}\right). \tag{4.83}$$

These assumptions are supported by measurements in different avalanches and debris flows in nature, large scale, dry snow and artificial ping-pong ball avalanches, (see, e.g., [3, 20, 64, 81]) as well as by small scale laboratory granular avalanches [21]. A detailed investigation on it will be given in Section 10.3.4

Note: *Consider the depth-averaged u component of the velocity and form*

$$\overline{u^2} = \frac{1}{h}\int_b^s u^2 dz = \alpha_1 \overline{u}^2, \tag{4.84}$$

where α_1 is a constant emerging from the integration operation. Values of α_1, in this equation, which deviate from unity give information about the deviation of the velocity profile from uniformity. For example for a parabolic velocity profile with vanishing basal

velocity (corresponding to no sliding and all differential shear) $\alpha_1 = 6/5$ *whereas for a uniform profile (all sliding and no differential shear)* $\alpha_1 = 1$. *Since it is likely that sliding is present, the active shear zone is confined to a thin basal layer and the velocity profile is blunt [83]. So, without introducing a large error one may choose* $\alpha_1 \approx 1$. *This justifies the presence of the* $O(\varepsilon^{1+\gamma})$*-term in (4.82) and (4.83).*

4.9 Model Equations in Conservative Form

In this Section we present the final form of the model equations in conservative form that can be used to describe the avalanche and debris motion down arbitrarily curved and twisted channels. We will also make it clear about how the new model equations can exactly be reduced to the previous model equations of the SH-theory. Moreover, we will outline some importance of the new model equations. Finally, we will compute the characteristic speeds and critical flows by introducing the standard conservative form of the model equations.

4.9.1 Avalanche Motions Down Curved and Twisted Channels

With (4.82) the mass balance equation (4.69) reduces to

$$\frac{\partial h}{\partial t} + \frac{\partial}{\partial x}(hu) + \frac{\partial}{\partial y}(hv) = 0 \tag{4.85}$$

which is correct to order $O(\varepsilon^{1+\gamma})$. Moreover, with the results (4.80)–(4.81) and (4.82)–(4.83), the depth-integrated downslope and cross-slope momentum balances (4.70)–(4.71) yield

$$\frac{\partial}{\partial t}(hu) + \frac{\partial}{\partial x}\left(hu^2\right) + \frac{\partial}{\partial y}(huv) = hs_x - \frac{\partial}{\partial x}\left(\frac{\beta_x h^2}{2}\right), \tag{4.86}$$

$$\frac{\partial}{\partial t}(hv) + \frac{\partial}{\partial x}(huv) + \frac{\partial}{\partial y}\left(hv^2\right) = hs_y - \frac{\partial}{\partial y}\left(\frac{\beta_y h^2}{2}\right), \tag{4.87}$$

again correct to order $O(\varepsilon^{1+\gamma})$, where the superscript, 'b' is dropped. The factors β_x and β_y are defined as

$$\beta_x = -\varepsilon g_z K_x \quad \text{and} \quad \beta_y = -\varepsilon g_z K_y, \tag{4.88}$$

respectively. The terms s_x and s_y represent the *net driving accelerations* in the downslope and cross–slope directions, respectively, and are given by

$$s_x = g_x - \frac{u}{|\mathbf{u}|}\tan\delta\left(-g_z + \lambda\kappa\eta u^2\right) + \varepsilon g_z \frac{\partial b}{\partial x}, \tag{4.89}$$

$$s_y = g_y - \frac{v}{|\mathbf{u}|}\tan\delta\left(-g_z + \lambda\kappa\eta u^2\ \right) + \varepsilon g_z \frac{\partial b}{\partial y}, \tag{4.90}$$

where $|\mathbf{u}| = (u^2 + v^2)^{1/2}$ is the magnitude of the velocity field tangential to the reference (basal) topography and $\eta = \cos(\theta + \varphi(x) + \varphi_0)$, $\zeta = \sin(\theta + \varphi(x) + \varphi_0)$ and $\theta = y/(\varepsilon z_T)$.

The first terms on the right–hand side of (4.89) and (4.90) are due to the gravitational acceleration. The second terms of both equations emerge from the dry COULOMB friction, the third terms are the projections of the topographic variations along the normal direction.

Given the basal topography b, the material parameters δ and ϕ, equations (4.85)–(4.87), which are written in non-dimensional form and constitute a *two-dimensional conservative system of equations*, allow three independent variables h, the avalanche geometry, and u and v, depth-averaged bed-parallel velocity components in the longitudinal and lateral directions, respectively, to be computed as functions of time and space, once appropriate initial and boundary conditions are prescribed.

4.9.2 Importance of the New Theory

(I) Reduction to the Previous Models

The present theory can directly be reduced to the previous models of the SAVAGE-HUTTER theory. Note that in applications and numerical computations, it is convenient to take the sign of g_z to be negative which corresponds to the upward pointing normal from the talweg. With this convention, the model equations, (4.85)–(4.90), can exactly reproduce the previous equations of GRAY et al. [31] as a special case. We want to prove this fact in the following paragraphs.

For this purpose we consider a basal topography which is curved in the down-slope direction as described by the following mathematical representation:

$$\tilde{\zeta}(x) = \begin{cases} \tilde{\zeta}_0, & 0 \le x \le x_l \\ \tilde{\zeta}_0 \left(\dfrac{x_r - x}{x_r - x_l} \right), & x_l \le x \le x_r \\ 0, & x \ge x_r, \end{cases} \tag{4.91}$$

where $\tilde{\zeta}_0$ is the inclination angle[‖] of the straight upper part of the reference surface which merges continuously into a horizontal run-out plane as shown in Fig. 4.10a. In this figure and the corresponding equation, x_l and x_r are the left and right end points of the continuous transition connecting the two straight parts, an upper inclined and another horizontal part, respectively. If the topography is flat laterally, we consider the azimuthal angle θ to be very small and the distance between the reference curve and the talweg, $0\tilde{0} = z_T$, relatively large. Then, the components of the gravitational acceleration in the down-slope, cross-slope and the normal directions of the basal topography, respectively, are given by

$$\begin{aligned} g_x &= \sin\tilde{\zeta}, \\ g_y &= 0, \\ g_z &= -\cos\tilde{\zeta}. \end{aligned} \tag{4.92}$$

Furthermore, when the topography is flat in the lateral direction it is then torsion free, so that $\varphi(x) = 0$. We take the value of φ_0 (which in the derivation of the theory is an

[‖]Note that $\tilde{\zeta}$ here corresponds to ζ in Chapter 3

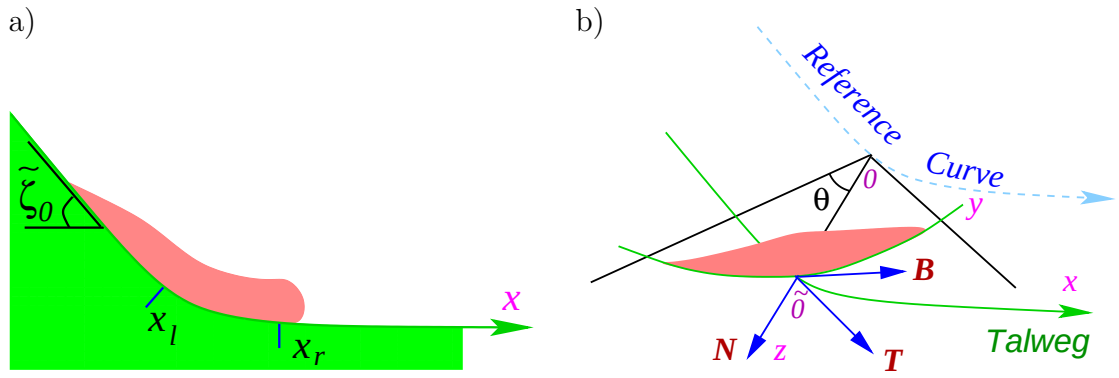

Figure 4.10: a) Avalanche passing through the transition into the run-out zone in a vertical plane containing the talweg of the valley. In this picture, x_l and x_r are the left and right end points of the continuous transition between the straight inclined upper part with inclination angle $\tilde{\zeta}_0$ and horizontal run-out in the valley. b) For a given value of the arc length, the avalanche domain in the lateral direction occupies a region in a circular section of a plane perpendicular to the talweg of the valley and θ is the azimuthal angle in this plane. The depth of the avalanche in this section is represented by a height function (of the avalanche) which at different positions are not parallel but radial. $O\tilde{O} = z_T$ is the radial distance between the master (reference) curve and the talweg. The lateral coordinate, y, is determined by the transformation $y = \theta z_T$. $\{\mathbf{T}, \mathbf{N}, \mathbf{B}\}$ is the moving orthonormal unit triad following the talweg (equivalently the master curve). $\tilde{\zeta}$ is the slope angle of the talweg with the horizontal

arbitrary constant) to be zero. Thus, we have the following additional conditions corresponding to the restricted topography considered previously by Gray et al., Wieland et al. [31, 131], and many others:

$$\theta = 0, \quad \varphi(x) = 0, \quad \varphi_0 = 0, \quad \eta = 1, \quad \zeta = 0. \tag{4.93}$$

With conditions (4.92) and (4.93), the model equations presented in Section 4.9.1 can exactly reproduce all previous model equations of the Savage-Hutter-theory as mentioned in Section 3.3.3. Therefore, the theory presented in this Chapter, which can be applied to arbitrarily curved and twisted mountain topography and channels in industrial flow configurations, is very important both from the theoretical and application point of view.

(II) Special Features of the New Theory

For the last thirteen years, the *SH*-theory was *only directly generalised* from the one-dimensional configuration to the quasi-two-dimensional flow situations in which the talweg of the topography varies only in the vertical plane. Pudasaini & Hutter [101] started the derivation of the new theory from a *completely different geometrical point of view* in which not only the talweg but also the entire basal topography can be curved and twisted. Although this new theory was started from quite a different topographical and analytical setting, the model equations can directly be reproduced to achieve all previous relatively simple and restricted model equations.

If we consider the model equations derived by Gray et al. [31], we immediately see that there is no mechanism which could produce and represent the sidewise component of the gravitational acceleration for a channelised flow. This means that their model equations can, in general, not be applied to a channelised flow, of which the talweg is a plane curve in a vertical plane. To model the channelised flow they superimposed a basal topography,

which enters into the model equations through the kinematic boundary conditions and the depth-integration procedure. But there is no term in the final governing equations which can replace the sidewise component of the gravity force in a fundamental way. If the sidewise bent of the channel is strong, the lateral component of the gravity turns out to be a very important factor to force the mass to concentrate along a small longitudinal vicinity of the talweg. This drawback is eliminated in the new model equations proposed by PUDASAINI & HUTTER [101]. The physics of the sidewise motion of the avalanche is modelled by a systematic inclusion of the gravitational acceleration component in the lateral direction, e.g., g_y, in the first term on the right-hand side of the net driving force, (4.90), in the cross-slope direction. Due to the topographic restriction, this lateral component of the gravity force always remained zero, $g_y = 0$, in the model equations derived by GRAY et al., and all previous model equations. The effect of the term g_y on the dynamics of avalanche is discussed more explicitly in Section 8.3.2

4.9.3 Standard Form of the Differential Equations

Definition: *A system of partial differential equations is said be in conservative form if it can be written as*

$$\frac{\partial \mathbf{w}}{\partial t} + \frac{\partial \mathbf{f}\,(\mathbf{w})}{\partial x} + \frac{\partial \mathbf{g}\,(\mathbf{w})}{\partial y} = \mathbf{s}\,(\mathbf{w}), \tag{4.94}$$

where $\mathbf{w}$*,* $\mathbf{f}$*,* $\mathbf{g}$ *and* $\mathbf{s}$ *are vector valued quantities. Otherwise it is said to be in non-conservative form.*

Now, we will write the *two-dimensional conservative system of equations* (4.85)-(4.87), with the specifications (4.88)-(4.90), in the general and "compact" vector form (4.94) where $\mathbf{w}$ denotes the vector of the *conservative veriables* and $\mathbf{f}$, $\mathbf{g}$ represent the *transport fluxes* in the x- and y-directions, respectively. Similarly, $\mathbf{s}$, on the right-hand side of the equation represents the vector of the source terms. Let us define the conservative variables as h, $m_x = hu$ and $m_y = hv$. Then, the model-equations (4.85)-(4.87) can be written in the form (4.94), where $\mathbf{w}$, $\mathbf{f}$, $\mathbf{g}$ and $\mathbf{s}$ are given by

$$\mathbf{w} = \begin{pmatrix} h \\ m_x \\ m_y \end{pmatrix},\ \mathbf{f} = \begin{pmatrix} m_x \\ m_x^2/h + \beta_x h^2/2 \\ m_x m_y/h \end{pmatrix},\ \mathbf{g} = \begin{pmatrix} m_y \\ m_x m_y/h \\ m_y^2/h + \beta_y h^2/2 \end{pmatrix},\ \mathbf{s} = \begin{pmatrix} 0 \\ h s_x \\ h s_y \end{pmatrix}. \tag{4.95}$$

The values of the terms β_x, β_y, s_x and s_y must be carried over from (4.88)-(4.90).

4.9.4 Characteristic Speeds and Critical Flow

In order to compute the characteristic speeds of the system of equations (4.94) and (4.95), we rewrite it as

$$\frac{\partial \mathbf{w}}{\partial t} + \mathbf{A} \begin{pmatrix} \dfrac{\partial \mathbf{w}}{\partial x} \\ \dfrac{\partial \mathbf{w}}{\partial y} \end{pmatrix} = \mathbf{s}, \quad \mathbf{A} = (\mathbf{A}_x,\ \mathbf{A}_y)\,, \tag{4.96}$$

where

$$\mathbf{A}_x := \frac{\partial \mathbf{f}}{\partial \mathbf{w}} = \begin{pmatrix} 0 & 1 & 0 \\ -m_x^2/h^2 + \beta_x h & 2m_x/h & 0 \\ -m_x m_y/h^2 & m_y/h & m_x/h \end{pmatrix},$$
$$\mathbf{A}_y := \frac{\partial \mathbf{g}}{\partial \mathbf{w}} = \begin{pmatrix} 0 & 0 & 1 \\ -m_x m_y/h^2 & m_y/h & m_x/h \\ -m_y^2/h^2 + \beta_y h & 0 & 2m_y/h \end{pmatrix}. \tag{4.97}$$

The characteristic speeds are only defined in a spatially one-dimensional situation. To achieve this at a fixed position $\mathbf{x} = (x, y)$ in the avalanche a rotation of the coordinate system must be performed such that in the rotated coordinate system (identified by the asterisks) equation (4.96) reduces to

$$\frac{\partial \mathbf{w}^*}{\partial t} + \mathbf{A}^* \begin{pmatrix} \dfrac{\partial \mathbf{w}^*}{\partial x^*} \\ \mathbf{0} \end{pmatrix} = \mathbf{0}, \quad \mathbf{A}^* = \left(\mathbf{A}_x^*,\ \mathbf{A}_y^*\right) \tag{4.98}$$

implying that the characteristic equation is now given by

$$\det\left(\mathbf{A}_x^* - \lambda \mathbf{I}_3\right) = 0. \tag{4.99}$$

Note that the condition $\partial \mathbf{w}^*/\partial y^* = \mathbf{0}$ defines the rotation matrix $\mathbf{O}$ of the coordinate system.

We restrict ourselves for this discussion to the situation for which this rotation does not have to be performed, namely those lines for which either $\partial \mathbf{w}/\partial y = 0$ or else $\partial \mathbf{w}/\partial x = 0$. Equation (4.99) then reads

$$\det\left(\mathbf{A}_x - \lambda \mathbf{I}_3\right) = 0, \quad \text{and} \quad \det\left(\mathbf{A}_y - \lambda \mathbf{I}_3\right) = 0 \tag{4.100}$$

with the solutions

$$\lambda_1 = u, \quad \lambda_{2,3} = \frac{m_x}{h} \pm \sqrt{\beta_x h},$$
$$\lambda_4 = v, \quad \lambda_{5,6} = \frac{m_y}{h} \pm \sqrt{\beta_y h}. \tag{4.101}$$

$\lambda_{1,4}$ give as characteristic speed the particle velocity in the x- and y-directions, respectively; alternatively, the other solutions give in each case a subcritical and supercritical speed in the x- and y-directions, respectively. The general case explained by (4.96) will also yield these solutions.

When a finite avalanching mass of granular material moves down a steep slope and approaches the runout zone with a supercritical speed, a considerable deceleration will suddenly occur and lead to a transition from supercritical to subcritical flow. Any such transition from a *supercritical* to a *subcritical* flow state produces a shock as shown in Fig. 2.3 and described in its caption. That is accompanied with changes from small heights and larger speeds to larger heights and smaller speeds. In this thesis, we will develop and implement shock capturing numerical schemes for this system. An explicit analysis is given in Chapters 6 and 7.

4.10 Discussion

4.10.1 Summary and Embedding Earlier Models

Equations (4.85)–(4.87) with the precisions (4.88)–(4.90), or the equivalent system (4.94)–(4.95), comprise a hyperbolic system of equations for three unknown field quantities, h, u and v; these are representative for an avalanche thickness and down- and cross-slope thickness averaged velocity components. The equations are formally analogous, almost identical, to those of previous derivations under (much) simpler situations, see Savage & Hutter, Gray et al. and Wieland et al. [31, 112, 113, 131]. For $\eta = 1$ and $\zeta = 0$, which correspond to a large distance between the master curve and the talweg and a small azimuthal angle in the cross-sectional plane, these equations reduce to those of Gray et al. and Wieland et al.

By varying the azimuthal angle and the distance between the talweg and the master curve it is now possible to analyse the motion of avalanches in channels with different cross-sections. Another major advantage of these new model equations is that they include the effect of torsion in the avalanching motion, which could not be achieved by other previous models. Therefore, the applicability of the present model equations is by far broader than in the previous cases. This has been achieved by use of a different underlying coordinate system.

Obviously, for different azimuthal angles the radial directions are not parallel; at this point the present model deviates from previous ones. It implies that the earlier equations of the SH-model with torsion free master curves are exactly reproduced when these master curves are moved far away. Practically, the master curve does not need to be moved infinitely far away from the talweg; it suffices if $z = b(x, y, t) = O(\varepsilon^{-1-\eta})$, $\eta > 0$ to obtain numerical coincidence.

The *careful derivation* of the model was important because it delineates the applicability of the model by explicitly stating the underlying simplifications. These are similar to those already imposed in the original SH-equations [112, 113]. They are explicity stated in the introduction and primarily pertain to *shallowness* and *small curvature* but also involve a significant *principal stress assumption* on the basis of which downslope shearing in planes parallel to the basal surface is dominant. With this assumption the rotational invariance of the original equations is not maintained by the model equations, but this is no significant restriction, since avalanches primarily move down-hill with small transverse spreading. A further important underlying assumption of the model is the *uniformity with depth of the downslope and cross slope velocity components*. There is limited observational evidence

under simpler conditions both in the field (Dent et al., Keller et al., McElwaine & Nishimura [20, 64, 81]) and the laboratory (Eckart, Gray & Hutter [21]) providing support for this assumption. This will also be discussed in Section 10.3.4. Incidentally, the assumption is popular in fluid mechanics and corresponds to the neglect of the correlation integrals of velocity differences from uniformity akin to the omission of the Reynolds stresses in turbulence theory. This analogy, however, is merely formal with no physical bearing to turbulence. Assuming power law distributions of the velocity with depth will show that $\overline{u^2} = \alpha\,(\overline{u})^2$ with $1 \leq \alpha \leq 1.2$ where the upper value applies for a parabolic distribution. Measured velocity profiles are much closer to uniformity than parabolas (see, [21]) and so α is very close to unity.

The underlying assumptions described above are important ingredients of the model to reduce the governing partial differential equations to conservation form. They eliminate all those Christoffel symbols that would "destroy" the conservation property of the emerging equations. This is mathematically and numerically pleasing since established methods exist for conservation equations to prove existence of solutions and convergence of numerical integration schemes including those of *front–tracking* and *shock capturing*. In spite of this, equations (4.94)–(4.95) are still a challenge both to mathematical and numerical analysts. The equations involve a coefficient (e.g., the earth pressure coefficient) which may be discontinuous when the flow changes from diverging to converging conditions or vice versa. To our knowledge, mathematicians are still trying to prove the existence of solutions under such general prerequisites.

Nevertheless for strictly diverging flow conditions the equations allow the construction of restricted similarity solutions analogous to those originally already constructed by Savage & Hutter [112]. Such parabolic cap and M-wave solutions are explicitly presented by Pudasaini et al. in [98, 99]. We believe them to be important despite their simplicity and similarity to the corresponding Savage–Hutter solutions because they demonstrate well posedness under at least restricted conditions and may, furthermore, be used to partly verify a code for their numerical integration [121]. For simple cases slope stability analysis and the translational motion also present some further physical meanings and pave a way to compare the present models with other previously existing model equations, as shown by Pudasaini & Hutter [100]. A detailed investigation on it is given in [105].

At this point it is worthwhile to have a systematic comparison of the model equations of this Chapter with the previously developed model presented in the last Chapter.

4.10.2 Orthogonal Complex Versus Orthogonal General System

In situations when the talweg is a plane curve in a vertical plane, it is already proven (for instance, see [31, 131]) that this system, called the *orthogonal complex system* can reproduce laboratory experiments to a very good approximation. The equations derived in these papers were also used to reproduce the flow of a granular avalanche down a channel with slowly meandering talweg with fair to good agreement of experimental and computational findings [30]. All this is demonstrated in [105]. The major problem in extending this model was to introduce non-uniform curvature *and* torsion in the metric that describes the whole flow behaviour. It is made possible by using the *orthogonal general system* of equations derived in this Chapter. In many cases the orthogonal complex

system seems to be very useful. Nevertheless, in general, the orthogonal general system may serve as a good theoretical foundation in order to investigate the flow of granular masses in more complicated topographies. Here, we discuss the connection and differences between these two theories.

- **Broad Applicability** The general equations (4.85)–(4.87) with the specifications (4.88)–(4.90) are analogous to previous derivations (3.18)–(3.20), also see [31, 47, 131]. However, this general system of equations can be applied over a large variety of topographies. It is made possible by the choice of an arbitrarily varying orthogonal coordinate system along the talweg of the valley than in the previous models. For this reason, there is no limit of these new model equations to be used in realistic flow situations both in nature and in industrial applications.

- **Introduction of Non-Uniform Curvature and Torsion** The key idea was the use of an orthogonal curvilinear moving coordinate system that is based on a master line in three-dimensions which exhibits *non-uniform curvature and torsion*. The talweg of a valley (possibly shifted a certain distance in the normal or vertical direction) or the axis of a three dimensionally curved and twisted channel or pipe may be the basis for the construction of this master curve. Planes perpendicular to this master curve give rise to the introduction of a polar coordinate system within these planes, of which the origin is the intersection point with the master curve. The topographic profile of the avalanche within these planes can be described in terms of these polar coordinates; the normal (radial) direction determines the direction of the height, the cross–slope (azimuthal) direction embraces its width. A shift in the normal coordinate makes it possible to bring the origin of the coordinate system down in the valley at a point in the talweg.

- **Flexible and More Realistic** The advantage of the formulation of a model of depth-integrated avalanche equations of this Chapter lies in its flexibility of application. The flow down an inclined plane or within a channel of which the axis lies in a vertical plane but may be curved and the flow of a granular avalanche in a helicoidal channel of arbitrary cross section can be described as can the flow down mountain valleys with arbitrarily curved and twisted talwegs. It is this last application which has motivated us to derive this model, because it is ideally suited to the application in realistic situations in connection with the use of *Geographical Information and Visualisation Systems* (GIVS).

4.11 Concluding Remarks and Future Outlook

The above discussion should have made convincingly clear that the proposed model equations (4.85)–(4.87) are suitable for the prediction of avalanche flows of granular materials down arbitrarily curved and twisted tracks. Since the equations reduce to earlier models for which the Savage-Hutter-theory has been demonstrated to well reproduce results from laboratory experiments, there is no question about the validity and the applicability of the new theory. The theory presented in this Chapter is to date *the most sophisticated and the most advanced theory* in the field of avalanche research. The model equations have unlimited applications in geophysical and industrial avalanches of flow type.

The next and immediate goal for researchers interested in this field may be to perform numerical simulations with the intention to provide a general purpose software for practitioners involved with the prediction of avalanche run-out in mountainous regions. The intention should be the use of *Geographical Information Systems* (GIS) from which digitised realistic topographies in mountainous regions are available. With these GIS particular avalanche-prone subregions can be selected and for individual sites the master curve and the cross sectional topography constructed. From a preselected release of a finite mass of gravel or snow at a breaking zone it is then intended to determine the flow from initiation to run-out. This step requires numerical integration via an avalanche purpose software using total-variation-diminishing non-oscillating schemes. Its output can, in a final step, be used in visualisation software to identify endangered zones. A multitude of applications will then be at the disposal for practitioners to be investigated with the software. Needless to say that comparison with observational data in the field taken by photography from helicopters and airplanes, or digital video cameras positioned at a fixed station, or the satellite data, then become possible.

Chapter 5

Flow Through a Helicoidal Channel

5.1 Motivation

From a pure engineering and practical applications point of view it is sometimes better to derive equations for some avalanche model which are specially designed to a particular topographic situation. This then restricts the applicability of the model equations to that particular case. At this point we would like to test whether the concept of the Savage-Hutter-theory can be applied for the derivation of avalanche-model equations for a very special case so as to initiate further investigations for particular geometry. One such interesting case is as follows: In the transportation of solid materials a finite mass of a dry granular material may have to be transported through a channel with helicoidal surface, see Fig. 5.1. For instance, one may consider the flow of capsules or pills in the pharmaceutical industries, cereals in the agricultural and food producing industries, and powder substances in chemical process engineering through such channels. One may then ask: why are we considering this type of special topography? The answer is quite simple and threefold: (i) Such a model may serve as one of the most simple mathematical and analytical representations of a basal topography which simultaneously includes curvature and torsion effects into the analytical description of the avalanche as it slides down along the channel. (ii) Helicoidal surfaces are widely used in industrial and technical applications. (iii) Some model equations may be "easy" to develop but when they have to be validated by some realistic laboratory experiments or field data this may turn out to be very complicated. Therefore, before starting the development of some model equations one must always keep in mind the question: Can we reproduce the theory, at least, in the laboratory? Otherwise, the whole work is, so to say, "worthless!". For this reason we consider a helicoidal geometry of the bed and make use of a non-orthogonal metric which allows relatively easy comparison with laboratory experiments. It will turn out that the fundamental hyperbolic structure of the equations remains preserved.

5.2 Introduction

In this Chapter we will present another important extention of the the SH–theory to rapid *shear flows* of dry granular masses in a *curved* and *twisted* channel having both *curvature* and *torsion*, by Pudasaini, Eckart & Hutter [99]. In particular, we deal with a *helicoidal surface geometry*. The motion of the avalanche follows the helicoidal talweg.

This theory is aiming to provide evidence that the SH–model works well not only for topographies having curvature in one direction but also for rather strongly curved chutes having curvature as well as torsion. Different from the original SH–theory [112, 113], we choose *helicoidal coordinates* and use them to define a curvilinear coordinate system. In contrast to other previous extensions, this local coordinate system is based on a generating curve, namely a helix, with curvature and torsion. As in the SH–model, we formulate the balance laws of mass and momentum as well as the boundary conditions in terms of these coordinates, average these equations over depth and then non-dimensionalise the averaged equations. There is, however, a difference in *non-dimensionalising* the equations and in the *ordering analysis* as compared to the original theory. The depth of the avalanche is defined in a *new* way; it is taken parallel to the direction of the gravitational acceleration. This is in contrast to the previous works. Traditionally, it was taken to be normal to the basal topography. The final governing balance laws of mass and momentum appear to be much less complicated with the averaging operation performed vertically to the basal surface than perpendicularly. It is clearly due to the use of a *non-orthogonal basis*.

The rigorous mathematical computations and the physical reasonings are analogous to the theorem presented in Chapter 4. Therefore, here, we will only present a short review of the theory. For detail study, we refer to [99].

5.3 Non-Orthogonal Helical Coordinate System

Let us consider a curved channel of which the talweg follows a helix with a given pitch. This helicoidal topography is sketched in Fig. 5.1a. It is therefore natural to consider curvilinear coordinates which follow this helicoidal geometry as closely as possible. For the ensuing analysis, let $\{\mathbf{e}_1, \mathbf{e}_2, \mathbf{e}_3\}$ be a Cartesian basis of the three-dimensional space $\mathbb{R}^3$. Then any point in $\mathbb{R}^3$, referred to this basis, can be represented by its position vector $\mathbf{r} = r_1\mathbf{e}_1 + r_2\mathbf{e}_2 + r_3\mathbf{e}_3$, or

$$\begin{pmatrix} r_1 \\ r_2 \\ r_3 \end{pmatrix} = (r_1, r_2, r_3)^T . \tag{5.1}$$

A curve and a surface in $\mathbb{R}^3$ can be represented by continuous one- and two-parameter functions $\mathbf{r} = \hat{\mathbf{r}}(x)$ and $\mathbf{r} = \hat{\mathbf{r}}(x, y)$ which will be assumed to be unique mappings from the parameter spaces described by x and $(x,\ y)$, respectively. For instance,

$$\mathbf{r} = \hat{\mathbf{r}}(x) := \begin{pmatrix} R\cos x \\ R\sin x \\ ax \end{pmatrix}, \qquad \mathbf{r} = \hat{\mathbf{r}}(x,\ y) := \begin{pmatrix} y\cos x \\ y\sin x \\ ax \end{pmatrix}, \tag{5.2}$$

describe a helix with a *pitch* parameter a on a cylinder with radius R, and a screw surface, respectively; x is the polar angle in the plane of the basis vectors $\mathbf{e}_1$ and $\mathbf{e}_2$, and the cylindrical axis coincides with the direction of the basis vector $\mathbf{e}_3$. y is the radial distance from the $\mathbf{e}_3$-axis. Coordinate lines on this surface are the helices with radius y ($0 \le x \le 2n\pi$, where $n \ge 0$ is a real number) and straight lines in the radial direction and parallel to the $(\mathbf{e}_1, \mathbf{e}_2)$-plane, ($x$ fixed; $0 < y < \infty$). It is geometrically obvious that

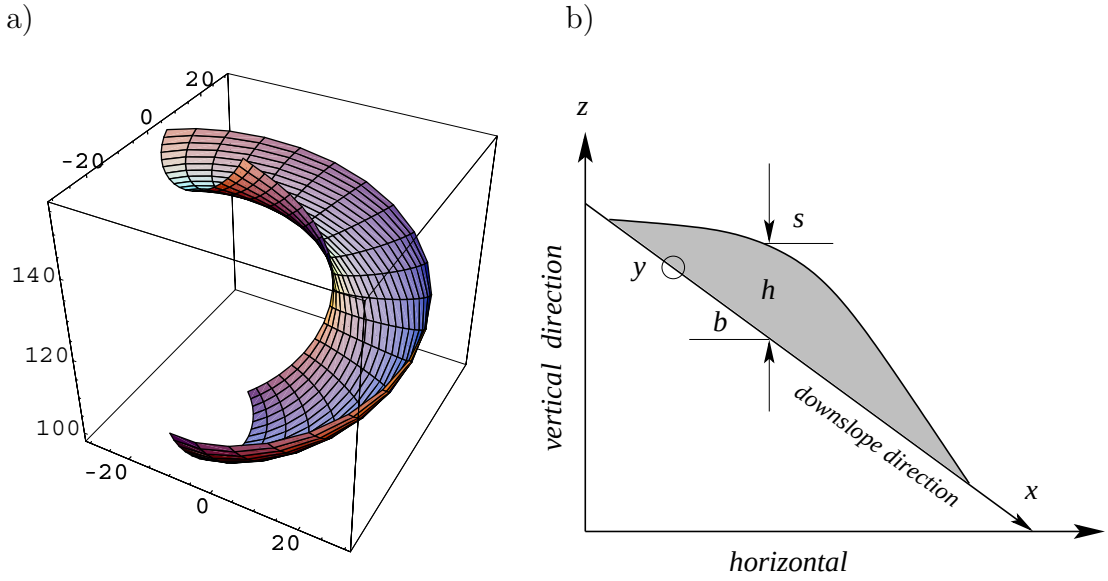

Figure 5.1: a) Helicoidal basal surface. The surface is embedded in a cube of which the edges are parallel to a Cartesian coordinate system. b) Depth integration along the direction of gravity

the entire space $\mathbb{R}^3$ is spanned by the three-parameter function

$$\mathbf{r} = \hat{\mathbf{r}}\,(x,\ y,\ z) := \begin{pmatrix} y\cos x \\ y\sin x \\ z + ax \end{pmatrix}. \tag{5.3}$$

Adding the coordinate z in the third component of $(5.2)_2$ generates, for fixed values of z, a screw-surface that is translated from the surface $(5.2)_2$ into the $\mathbf{e}_3$-direction by the distance z. It is geometrically trivial (it will become clear later) to see that not all coordinate lines of (5.3) are perpendicular to one another. So the corresponding metric is not orthogonal; this would be only the case for $a = 0$. The reader is warned that $(x,\ y,\ z)$ are *not* Cartesian components, but rather the coordinates of the helicoidal system. The tangent vectors to the coordinate lines, as shown in Fig. 5.2, are

$$\mathbf{g}_x = \begin{pmatrix} -y\sin x \\ y\cos x \\ a \end{pmatrix}, \quad \mathbf{g}_y = \begin{pmatrix} \cos x \\ \sin x \\ 0 \end{pmatrix}, \quad \mathbf{g}_z = \begin{pmatrix} 0 \\ 0 \\ 1 \end{pmatrix}. \tag{5.4}$$

These define the azimuthal, radial and vertical directions, respectively. The *covariant metric coefficients* are given by the matrix

$$(g_{ij}) = (\mathbf{g_i} \cdot \mathbf{g_j}) = \begin{pmatrix} y^2 + a^2 & 0 & a \\ 0 & 1 & 0 \\ a & 0 & 1 \end{pmatrix}. \tag{5.5}$$

The off-diagonal elements arising in the metric tensor, (5.5), are the manifestation of the *non-orthogonality* of the coordinates. The associated metric, for this system, is given by $ds^2 = d\mathbf{r} \cdot d\mathbf{r} = g_{ij}\, dx^i\, dx^j$, i.e.,

$$ds^2 = \left(y^2 + a^2\right) dx^2 + dy^2 + dz^2 + 2a\, dx\, dz. \tag{5.6}$$

The product term $2a\, dx\, dz$ corresponds to the *non-orthogonality* of the coordinate system under consideration.

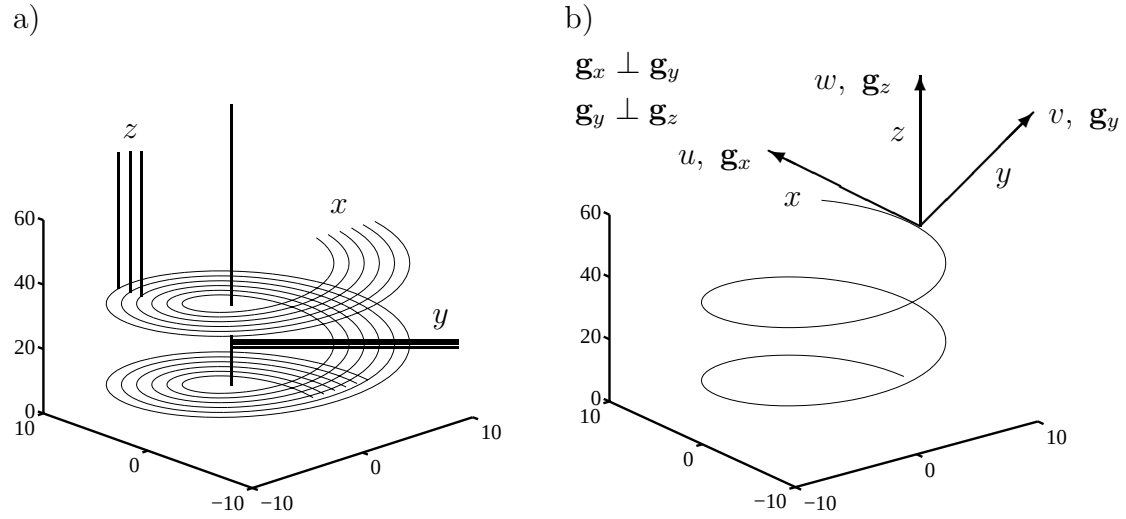

Figure 5.2: Sketch of the families of curves to generate a helically-ruled-surface. a) x is the polar angle of rotation, y measures the radial distance from the axis of the helix and z is the coordinate measuring the height parallel to the axis itself. The x, y and z coordinate lines are represented by curved and straight lines accordingly. A typical helix is given by $z = 0$ and $y = constant$. For $z = const.$ and variable values of x and y the emerging surface represents a helically-ruled reference surface (a surface generated by a *screw motion*) over which a basal topography $b = b(x, y, t)$ can be superimposed to form a curved and twisted channel, as shown in Fig. 5.1a. b) Arrows indicating the tangent vectors along the coordinate lines. Also shown are the components u, v, w of the velocity vector $\mathbf{u}$ along the coordinate lines x, y and z, respectively. The non-orthogonality of the coordinate system is indicated by the fact that the vectors $\mathbf{g}_x$ and $\mathbf{g}_z$ are not perpendicular to each other

5.4 The Governing Equations

As in the previous SH–model of Gray et al. [31], Pudasaini, Eckart & Hutter [99] have recently formulated the balance laws of mass and momentum as well as the boundary conditions of Section 3.3.1 in terms of the curvilinear helical coordinates of Section 5.3, averaged these equations over depth and then non-dimensionalised the averaged equations. There is, however, a slight difference in non-dimensionalising the equations and in the ordering analysis as compared to other previous theories associated with the orthogonal metric of the reference surface. The depth of the avalanche is defined in a new way; *it is taken parallel to the direction of the gravitational acceleration.* This is in contrast to the previous works. Traditionally (i.e., with orthogonal metric) it was taken to be normal to the basal topography. The final governing balance laws of mass and momentum appear to be much less complicated with the averaging operation performed vertically, see Fig. 5.1b. It is clearly due to the use of a non-orthogonal basis. This direction is also experimentally very convenient. For simplicity, it is also assumed that the basal surface b does not vary with the down-slope coordinate x, i.e., $\partial b/\partial x = 0$.

Conservative Form

With the aforementioned prerequisites, Pudasaini et al. [99] developed the following vertically averaged balance laws of mass; and momentum in the down-slope (azimuthal)

and cross-slope (radial) directions, respectively,

$$\frac{\partial h}{\partial t}+\frac{\partial}{\partial x}\left(\psi hu\right)+\frac{\partial}{\partial y}\left(hv\right)+\frac{h}{y}v=0, \tag{5.7}$$

$$\begin{aligned}\frac{\partial}{\partial t}\left(hu\right)+\frac{\partial}{\partial x}\left(\psi hu^2\right)+\frac{\partial}{\partial y}\left(huv\right)-\psi^2 hyuv+\frac{3h}{y}uv\\ =-\left(\frac{u}{|\mathbf{u}|}\tan\delta+\frac{a}{y}\right)h\chi-\varepsilon\psi\frac{\partial}{\partial x}\left(K_x\nu\frac{h^2}{2}\right),\end{aligned} \tag{5.8}$$

$$\begin{aligned}\frac{\partial}{\partial t}\left(hv\right)+\frac{\partial}{\partial x}\left(\psi huv\right)+\frac{\partial}{\partial y}\left(hv^2\right)+\frac{h}{y}v^2-\psi^2 hyu^2\\ =-\left(\frac{v}{|\mathbf{u}|}\tan\delta+\varepsilon\psi y\frac{\partial b}{\partial y}\right)h\chi-\varepsilon\frac{\partial}{\partial y}\left(K_y\nu\frac{h^2}{2}\right)\\ -\frac{\varepsilon}{y}\left(K_y\nu\frac{h^2}{2}\right)+\varepsilon\psi^2 y\left(K_x\nu\frac{h^2}{2}\right),\end{aligned} \tag{5.9}$$

where

$$\psi:=\frac{1}{\sqrt{y^2+a^2}},\ \ \nu:=1-\frac{2auv}{y\sqrt{y^2+a^2}},\ \ \chi:=\frac{y\sqrt{y^2+a^2}-2auv}{y^2+a^2}. \tag{5.10}$$

These equations appear here in *conservation form*. Equations (5.7)–(5.10) will henceforth be referred to as the *non-orthogonal helical equations*. The non-dimensional variables of system (5.7)–(5.10) can be mapped back to their dimensional form via the relations

$$\left(\hat{x},\hat{y},\hat{h},\hat{b}\right)=\left(x,Ly,Hh,Hb\right),\ \ \left(\hat{u},\hat{v}\right)=\sqrt{gL}\left(u,v\right),\ \ \hat{t}=\sqrt{L/g}t,\ \ \hat{a}=\mathcal{R}a. \tag{5.11}$$

The scalings (5.11) assume that the avalanche has a typical length-scale L tangential to the reference surface and a typical thickness H normal to it, and $\mathcal{R}$ is the stretching scale of the pitch of the helix. As before, the aspect ratio, ε, is assumed small. K_x and K_y are the earth pressure coefficients, as discussed in Section 4.7.

Finally, let us consider the down-slope (i.e., azimuthal) component of the momentum balance (5.8). This equation represents the *balance of change of momentum and the streamwise components of the net driving forces.* That is, the first two terms on the right-hand side are the friction force ($\tan\delta$) and a topographic effect, "a", together with the force associated with the overburden pressure (i.e. χ) at the base. The third term is the (collective) gradient of the earth pressure coefficient, overburden pressure and height of the pile. Similar inferences can be drawn for the cross-slope (radial) component of the momentum balance for which the final two terms are the contributions to the force due to the effects of the curvature and torsion of the topography, geometry of the moving pile and the earth pressure coefficients in two principal directions of the flow.

This system of three equations, (5.7)–(5.9), allows three variables h, u and v to be determined, once initial and boundary conditions are prescribed, provided the material parameters δ, ϕ, the pitch parameter a and the basal topography $b(x,y)$ are known.

Remark: *Before closing this section we ought to mention that the scalings required to arrive at the equations (5.7)–(5.10) are partly critically different from those of the original*

SH-theory, and these differences should be pointed out. The flow depth normal to the bed, $h_\perp$, and that vertically measured, h, are related to one another by the approximate relation $h = \sec\tilde{\zeta}\, h_\perp$ (where $\tilde{\zeta}$ is the local angle of inclination with the horizontal and this relation is based on the slow variation of the depth function with the longitudinal coordinate). Since the length scale remains unchanged, this corresponds to a change in the aspect ratio, ε, for this non-orthogonal case relative to that used for an orthogonal coordinate system, $\varepsilon_\perp$, namely $\varepsilon = \sec\tilde{\zeta}\,\varepsilon_\perp$. As long as $\tilde{\zeta} \in [0, 60°]$ we have $\sec\tilde{\zeta} \in [1, 2]$ which implies that ε and $\varepsilon_\perp$ are both of the same order of magnitude, typically $\varepsilon \in [10^{-3}, 10^{-2}]$.

More difficult seems the unchanged validity of the Earth pressure coefficients as referred to the internal and the bed friction angles, ϕ and δ. A straightforward geometric argument shows that the contravariant stress components p_{xy} may still be assumed to be small as compared to p_{xz} and p_{yz} so that the element faces with surface normals in the azimuthal direction are still primarily loaded by the pressures p_{yy} normal to these element faces (this is not so for p_{xx}). Provided we consistently work with the contravariant stress components, we then still can apply the earth pressure coefficients (see Section 4.7). However, the interpretation is then not exactly according to Mohr-Coulomb*, since they applied their yield condition to physical stress components. For small pitch the differences are also small.*

5.5 Conclusion

One may quickly infer that there are some direct connections between the two theories, non-orthogonal helical versus orthogonal general system, presented in this and the last Chapters. But, in general this is not the case. There are some connections and some major differences between them.

- **The Underlying Metric** It is clear from the model equations presented in this and the last two Chapters that the flows in any situation are characterised by the metrics and the topographies in use. Depending on some specific situations of investigations and the interest of the investigators, sometimes in particular a non-orthogonal helical system may be more applicable than the orthogonal general system. However in general, the latter may be more useful than the former.

- **Deduction of one System from Another** One thing in common may be that both of these systems should be able to produce similar results to some good approximation if we use simply a helix as a master curve in an orthogonal general system. This will have to be demonstrated by numerical computations and laboratory experiments.

- **Fundamental Differences in the Equations** Different ideas are used to derive these theories. The orthogonal general theory incorporates non-uniform curvature and torsion, whereas the helical system contains only curvature and torsion of a helix. This is one of the major differences between these two theories. Another difference concerns the depth integration. For the non-orthogonal helical system, the process of averaging along the direction of gravity is used which ultimately led the theory to a simple state. The theory would be much more complicated if we had not used this particular technique. For the orthogonal general system, the depth

integration along the normal of the basal surface is used which reduced the theory to simpler form. Many different realistic assumptions are made in order to generate these theories. One more example can be found in non-dimensionalising the physical variables. Non-dimensional parameters and ordering are also different for the two discussed theories.

- **Driving Force** At a first glance it seems that there is no component of the gravitational acceleration responsible for driving the motion along the helicoidal basal surface to the down-hill direction. It seems so, because the non-orthogonal coordinate system considered in (5.3) compels the gravity to act "totally" vertically in the negative direction of the gravitational acceleration. However, this is not a problem. Because, this then considerably increases the vertical pressure that is computed from the vertical component of the momentum balance equation. The driving force that is necessary to generate the motion is included in the model equations via the terms ν and χ in (5.10). The first term "1" on the right-hand side of ν is the manifestation of the fact that the gravitational force acts, in these model equations, via the vertical pressure. If the z coordinate of the coordinate system were not vertical but perpendicular to the reference surface this "1" would be replaced by "$1\cos\zeta$", where ζ is the local angle of inclination of the basal surface with the horizontal. This value is about $30-35\%$ larger (for ζ lying between 45° and 50°) than when referred to the orthogonal coordinate systems considered in Chapters 3 and 4. This excess force may be balanced by the second term of ν, i.e., "$-2auv/y\sqrt{y^2+a^2}$". Similar inferences can be made for χ. For more details on it, we refer to [99]. Because we are dealing with the helical coordinate system, the angle ζ is the angle between the tangent to the helix and the axis of the helix. It can be connected to the pitch parameter, a, of the helix by the relation $\tan\zeta = y/a$. Thus, the required force for the avalanching motion is generated by the joint effort of ν, χ and inclination angle ζ through the pitch parameter a.

All the three theories presented in Chapters 3, 4 and 5 are important in connection with the different configurations. Under some circumstances one may be better than the others. This is the main reason why we presented all of them and made a critical comparison among these different theories arising from different fundamental thinkings. Although all these systems work pretty well in the construction of semi-analytical solutions as discussed by Pudasaini and others in [98, 99, 100, 105], one can correctly conclude about the relationships among these theories only after performing some numerics and comparing them with relevant experiments and field data.